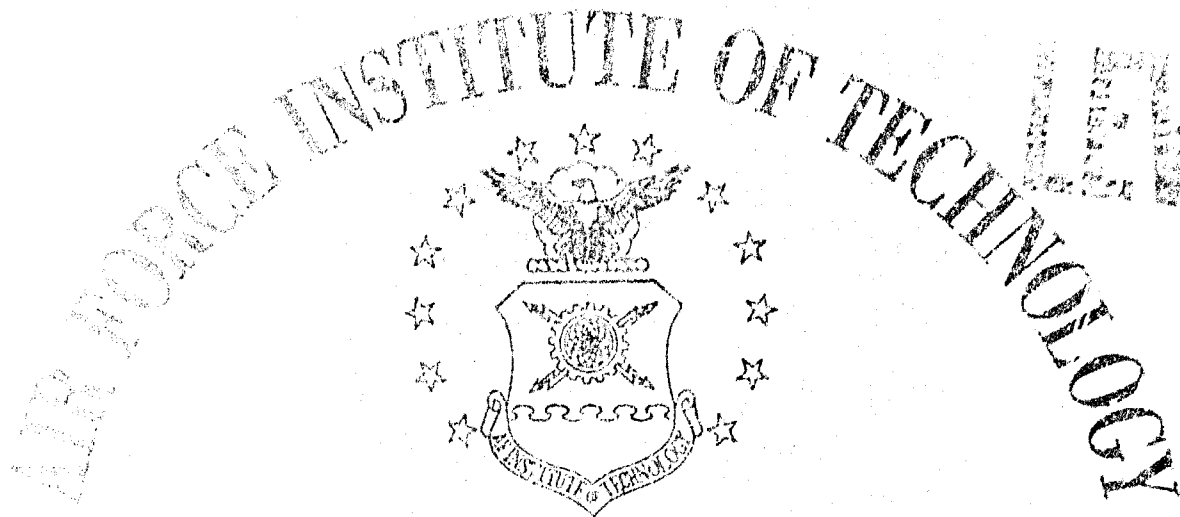
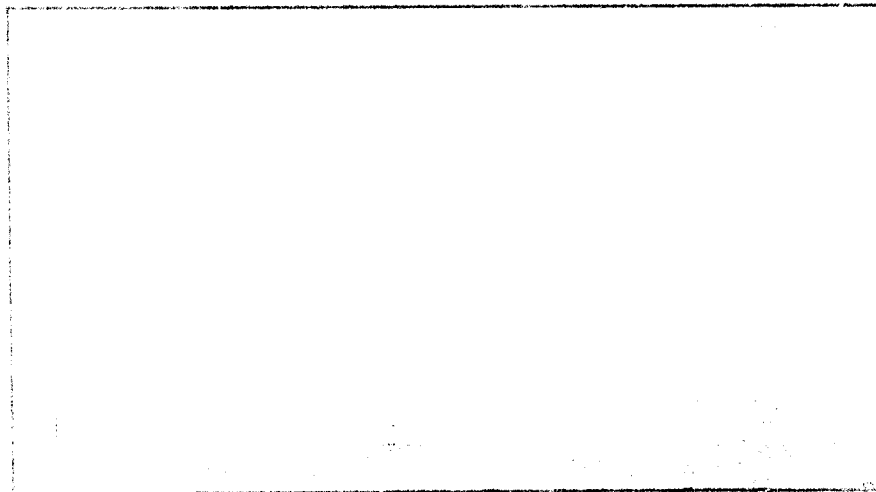


ADA 079857



AIR UNIVERSITY  
UNITED STATES AIR FORCE



SCHOOL OF ENGINEERING

D D C  
JAN 28 1980  
RECEIVED  
A  
DISTRIBUTION STATEMENT A  
Approved for public release  
Distribution Unlimited

WRIGHT-PATTERSON AIR FORCE BASE, OHIO

80 1 25 081

14

AFIT/GAE/AA/79D-7

ADA 079857

9 Master's Thesis,

6

AN EXPERIMENTAL STUDY OF STATIC  
THRUST AUGMENTATION USING A 2-D  
VARIABLE EJECTOR .

THESIS

AFIT/GAE/AA/79D-7

10

Eli Kedem  
Major, Israeli A/F

DDC FILE COPY

11

hloc 79

12

911

DDC  
R  
11/1/79

Approved for public release; distribution unlimited

012225

15

AN EXPERIMENTAL STUDY OF STATIC THRUST  
AUGMENTATION USING A 2-D  
VARIABLE EJECTOR

THESIS

Presented to the Faculty of the School of Engineering  
of the Air Force Institute of Technology

Air University

In Partial Fulfillment of the  
Requirements for the Degree of  
Master of Science

by

Eli Kedem, B.Sc.

Major Israeli A/F

Graduate Aeronautical Engineering

December 1979

Accession For	
NTIS	<input checked="checked" type="checkbox"/>
DDC	<input type="checkbox"/>
Unannounced	<input type="checkbox"/>
Justification	
By	
Distribution/	
Availability Codes	
Dist	Availability
A	Special

Approved for public release; distribution unlimited

## Preface

Studies of generating thrust augmentation by means of a jet ejector cover the past two decades. Nevertheless, due to the complicated flow mechanisms occurring in the ejector, namely, flow entrainment by viscous forces and energy transfer between flows, the theory of predicting an ejector performance has to rely heavily on data from experiments. The problem of developing a theory that can predict the performance of an ejector, is more acute in short ejectors, which are the ones needed to be incorporated into a VTOL aircraft's wing.

This study was done to contribute additional data on the design aspects and performance of a short ejector, which utilizes a center nozzle, coanda nozzles and BLC nozzles.

The ejector itself is highly variable (seven geometrical variables and three inlets with adjustable air supply) and can be used for additional investigation.

In order to accomplish this study I was helped by many, whom I want to thank. Many thanks to:

- Dr. Franke, my thesis advisor for his guidance and help.
- Dr. Nagaraja, my thesis sponsor, for his helpful remarks.

- Dr. Elrod and Dr. Wright, members of the Committee.
- Mr. Shortt, head of AFIT fabrication shop, Mr. Brohas and Mr. Murry, for their ingenuity in fabricating the ejector.
- Capt. Hayes and Mr. Baker for their help in the laboratory.
- Last but not least, my wife, Elana, and my two sons, Erel and Oren, that by their presence helped me to concentrate on my studies.

Eli Kedem

## Table of Contents

	Page
Preface . . . . .	ii
List of Figures . . . . .	vi
List of Tables . . . . .	viii
List of Symbols . . . . .	ix
Abstract . . . . .	xi
I. Introduction . . . . .	1
Jet Ejector Principle . . . . .	1
Coanda Effect . . . . .	3
Ejector and Nozzle Configurations . . . . .	4
Purpose and Objective . . . . .	6
Approach . . . . .	6
II. Apparatus . . . . .	8
The Ejector . . . . .	8
Air Supply System . . . . .	14
Instrumentation . . . . .	15
III. Experimental Procedures and Data Reduction . .	21
Thrust Equation . . . . .	21
Thrust Calibration of the Nozzles . . . . .	22
Data Reduction for Nozzle Thrust . . . . .	23
Primary Flow Calculations . . . . .	24
Total and Secondary Flow Calculations . . . .	24
IV. Results and Analysis . . . . .	26
Calibration Results of the Nozzles . . . . .	26
Center Nozzle . . . . .	26
Coanda and Diffuser Nozzles . . . . .	26
General Flow Phenomena . . . . .	30
Flow Phenomena in Unshrouded Ejector . . . .	31
Flow Phenomena in Shrouded Ejector . . . .	32

	Page
Thrust Augmentation Results . . . . .	34
Results for Unshrouded Ejector . . . . .	39
Results for Shrouded Ejector . . . . .	51
Ejector's Exit Flow Results. . . . .	54
V. Conclusions and Recommendations . . . . .	58
Nozzle Thrust Calibrations . . . . .	58
General Flow Phenomena Investigation . . . . .	59
Results from Unshrouded and Shrouded Ejectors . . . . .	59
Discussion of Future Testing . . . . .	61
Comparison of Ejector's Performances . . . . .	61
The Circular Ejector . . . . .	63
Bibliography . . . . .	67
Appendix A: Primary Flow Calculation . . . . .	68
Appendix B: Total Flow Calculation Program . . . . .	70
Vita . . . . .	81

## List of Figures

Figure	Page
1. Jet Ejector Principle . . . . .	2
2. The Coanda Effect . . . . .	3
3. Ejector Configurations . . . . .	5
4. Ejector Nomenclature and Variables . . . . .	9
5. Photograph of Unshrouded Ejector (Inlet View) . . . . .	10
6. Photograph of Unshrouded Ejector (Exit View) . . . . .	11
7. Inlet and Exit Vertical Shrouds . . . . .	14
8. Air Supply System . . . . .	15
9. Total and Static Pressure Taps . . . . .	17
10. Sketch of Ejector Installation . . . . .	18
11. Photograph of Ejector Installation . . . . .	19
12. Coanda and Diffuser Nozzle Thrust vs. Pressure Ratio . . . . .	27
13. Isentropic and Measured Coanda and Diffuser Nozzle Thrust Ratio vs. Pressure Ratio . . . . .	28
14. Thrust and Thrust Ratio vs. Pressure Ratio for End-Wall Nozzles . . . . .	29
15. Vortex Flow at Ejector Inlet . . . . .	31
16. Local Stall Region in the Ejector . . . . .	32
17. Reverse Flow . . . . .	33
18. Center Nozzle Jet's Stall . . . . .	34
19. $\phi_f$ for AR1 and $L_N/W1$ (Unshrouded) . . . . .	40
20. $\phi_f$ for AR1 and $L_N/W2$ (Unshrouded) . . . . .	41



# Figure

# Page

21.	$\phi_f$ for AR1 and $L_N/W3$ (Unshrouded) . . . . .	42
22.	$\phi_f$ for $L_N/W$ and AR1 (Unshrouded) . . . . .	43
23.	$\phi_f$ for AR2 and $L_N/W4$ (Unshrouded) . . . . .	44
24.	$\phi_f$ for AR2 and $L_N/W5$ (Unshrouded) . . . . .	45
25.	$\phi_f$ for AR2 and $L_N/W6$ (Unshrouded) . . . . .	46
26.	$\phi_f$ vs. $L_N/W$ for AR2 (Unshrouded) . . . . .	47
27.	$\phi_f$ vs. AR for $L_N = 2.5$ in. (Unshrouded) . . . . .	48
28.	$\phi_f$ and $\phi_i$ vs. MR for AR4 $L_N = 1.5$ in (Shrouded) . . . . .	52
29.	$\phi_f$ vs. MR for AR5 and AR6 (Shrouded) . . . . .	53
30.	Velocity Profiles . . . . .	55
31.	Nomenclature for Velocity Profile . . . . .	56
32.	Two Methods of BLC . . . . .	60
33.	Reduced Span of Primary Nozzle . . . . .	60
34.	Standard Test Apparatus--Suggestion . . . . .	62
35.	Circular Ejector . . . . .	63
36.	A Circular Ejector Application . . . . .	64
37.	A Circular Ejector Application . . . . .	66
38.	Coarse and Fine Data Matrices . . . . .	71
39.	Program EJECT Output . . . . .	77
40.	Program EJECT Output . . . . .	78

List of Tables

Table		Page
I.	Nozzle's Loss Coefficients . . . . .	24
II.	$\theta_{\max}$ VALUES . . . . .	35
III.	$L_N/W$ VALUES . . . . .	36
IV.	AR VALUES . . . . .	37
V.	DISTRIBUTION OF PRIMARY MASS FLOW VALUES . . . . .	38
VI.	CONSTANTS FOR PRIMARY FLOW . . . . .	69

### List of Symbols

A	Area ( $\text{in}^2$ ).
ARI	The I's throat/(Coanda and center nozzles) area ratio.
C	Conversion constant to match units. Not the same for all equations.
D	Main pipe diameter (in)
DPI	Pressure drop through the I's measuring orifice (in-Hg).
F	Thrust (lbf).
I	Index: 1-center, 2-coanda, 3-diffuser.
J	Factor of measuring orifice and pipe diameter ratio.
K	Nozzle's loss coefficient.
$L_E$	Length of ejector sidewall (in).
$L_N$	Length between throat and center nozzle (in).
$\dot{m}$	Mass rate of flow (lbm/sec).
P	Pressure (in-Hg)
PI	Upstream pressure in the I's supply pipe (in-Hg).
V	Velocity (ft/sec).
R	Gas constant (lb ft/slug $R^\circ$ ).
T	Temperature ( $^\circ R$ ).
W	Width of throat (in)
Y	Expansion factor.
$\alpha$	Angle between diffuser wall and mix wall (deg).
$\beta$	Skewness factor of flow.
$\gamma$	Ratio of specific heat.

$\rho$	Density (slug/ft <sup>3</sup> ).
$\theta$	Angle of coanda nozzle (deg).
$\psi$	Angle of mix sidewall (deg).
$\phi$	Thrust augmentation ratio.
1T	Total pressure at center nozzle (in-Hg gage).
2TU	Total pressure at coanda upper nozzle (in-Hg gage).
2TL	Total pressure at coanda lower nozzle (in-Hg gage).
3TU	Total pressure at diffuser upper nozzle (in-Hg gage).
3TL	Total pressure at diffuser lower nozzle (in-Hg gage).
4M	Total pressure at diffuser manifold nozzle (in-Hg gage).

#### Common Subscripts

a	Ambient
e	Nozzle exit.
f	Free.
i	Isentropic
I	Index: 1-center, 2-coanda, 3-diffuser.
j	Index of subarea at ejector exit.
p	Primary.
s	Static or secondary.
t	Total.
1	Center.
2	Coanda.
3	Diffuser.

### Abstract

A short rectangular throat ejector was constructed and tested to determine the effects of a number of variables on thrust augmentation and mass augmentation. The variables included those associated with geometry (e.g., diffuser length/throat length, diffuser area ratio, diffuser sidewall angle, nozzle angles and positions) and those due to differences in primary mass flow rate distributions among the nozzles.

There were two kinds of thrust augmentation that were calculated; the free thrust augmenting ratio and the isentropic thrust augmenting ratio. The free thrust augmenting ratio is the ratio of the ejector's measured thrust to the sum of the nozzles' measured thrust, if each of them were discharged separately to ambient pressure. The isentropic thrust augmenting ratio is the ratio of the ejector's measured thrust to the calculated thrust of the nozzles if discharged isentropically to the ambient pressure.

A free thrust augmenting ratio as high as 1.63 and an isentropic thrust augmenting ratio of up to 1.29 were obtained. Mass augmentation which is the ratio of secondary flow to primary flow was in the range of 3.5 to 5. Some conclusions concerning design aspects were drawn also. They include the necessity of 3-D shrouding for the

ejector's inlet and exit and the prevention of blowing high velocity air (primary and BLC flow) tangential to the ejector walls.

AN EXPERIMENTAL STUDY OF STATIC THRUST  
AUGMENTATION USING A 2-D  
VARIABLE EJECTOR

I. Introduction

One of the methods used to generate lift on a Vertical Take-Off and Landing (VTOL) aircraft involves an augmentor wing with a spanwise ejector. This allows an increase in the vertical thrust generated by the exhaust flow of the engine. Generally, this method, if optimized, enables the use of a smaller and more economical engine than that needed by other methods of vertical lift generators, like tilt wing, tilt propeller and vectored thrust.

Jet Ejector Principle

The jet ejector (Fig. 1) is a device in which a secondary, or driven, fluid is entrained by a primary, or actuating, fluid with subsequent transfer of energy through turbulent mixing. The primary fluid, which is originally at a higher stagnation pressure, is discharged with a high velocity into the mixing chamber of a specific shape. Due to viscous shear, the fluid surrounding the primary flow is brought into motion at the entrance of the mixing chamber. This motion causes a drop of static pressure, as

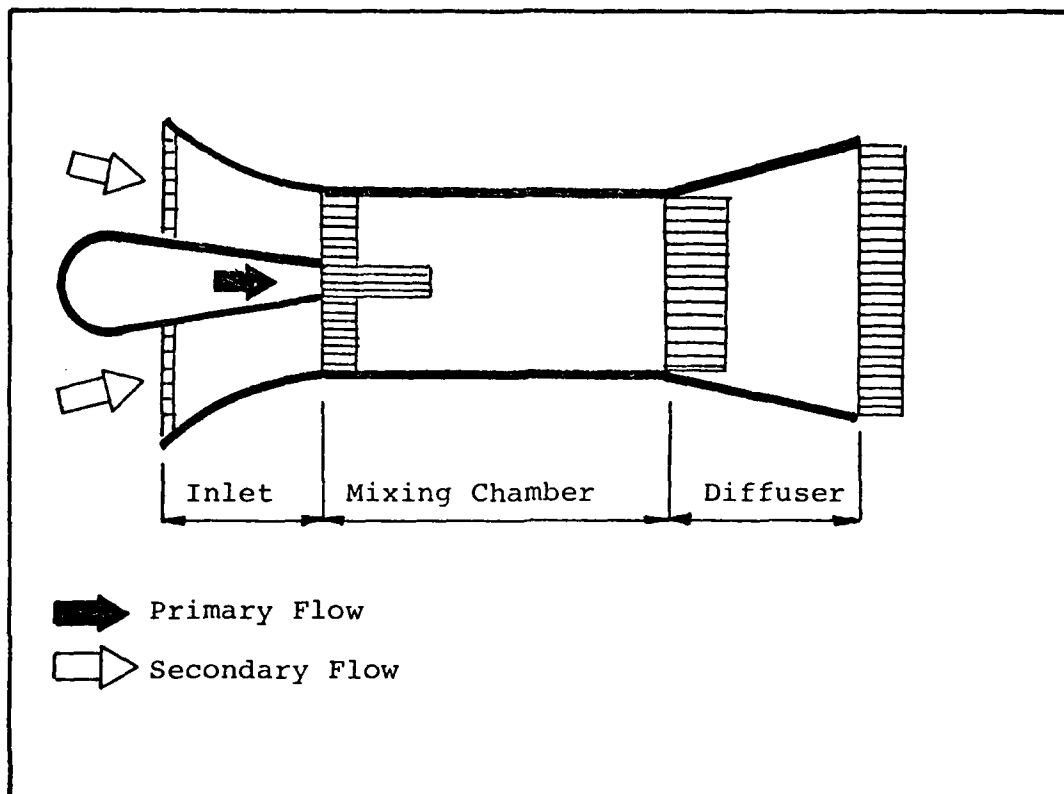


Fig. 1. Jet Ejector Principle

a result of which the secondary fluid (usually ambient air) is entrained into the mixing chamber. The secondary flow thus induced, mixes turbulently with the primary jet in the mixing chamber and in the diffuser and energy transfer occurs. The main function of the diffuser is to lower the pressure in the mixing chamber, thus enhancing the larger secondary flow. As a result of the pumping action as described above, the total momentum of the mixed flow at the ejector's exit is increased due to the entrainment of the secondary fluid, as compared with the momentum of the primary jet discharged isentropically



directly to ambient pressure. Jet thrust augmentation is thus achieved.

### Coanda Effect

The deflection of a plane wall jet by its adjacent boundary is called the Coanda effect (Ref 8). A plane wall jet, when blowing over a convex curved surface will remain attached to the curved surface through a considerable range of deflection angles. This capability is shown in Fig. 2. The attached jet also entrains mass from its surroundings because the pressure in the jet due to

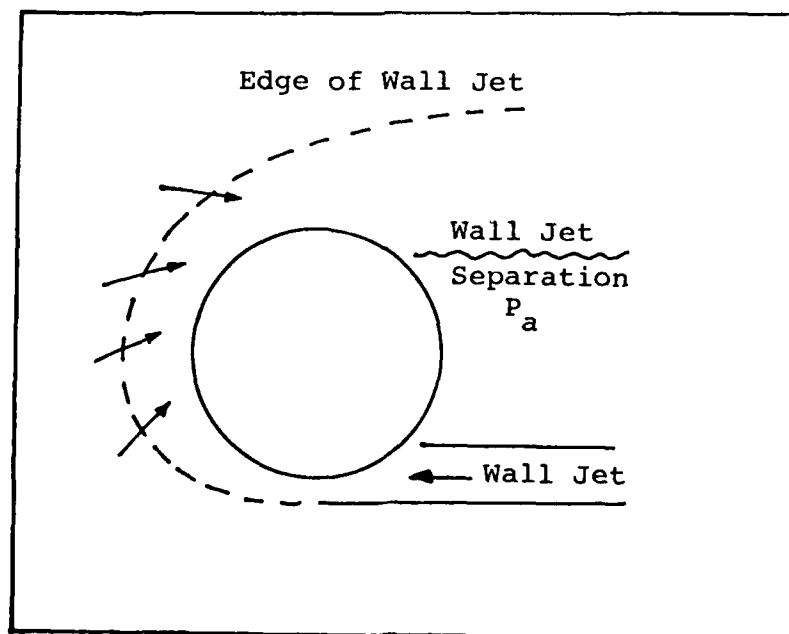


Fig. 2. The Coanda Effect (Ref 8)

flow curvature is less than the atmospheric pressure. Due to mass entrainment and viscous dissipation, the wall jet thickens, which in turn causes the wall jet pressure to increase. The wall jet finally entrains enough mass to cause the pressure to increase to approximately the ambient pressure. At this point the jet usually separates.

#### Ejector and Nozzle Configurations

In order to optimize the performance of ejectors, several approaches were used in various designs (Refs 4, 5, 6, and 7). Some of these ejectors and nozzles are shown in Fig. 3. The three main considerations in improving the performance of thrust augmenting ejectors are:

1. Enhancing the ratio of secondary to primary flow.
2. Increasing the amount of energy transfer between the primary and secondary flow.
3. Preventing stall in the diffuser.

These needs were met in the designs shown. For instance, the hypermixing nozzle and the cross slot nozzle increase the contact surfaces between the secondary and primary flow, thus increasing the amount of secondary flow and improving the energy transfer. The relative long and small angle diffuser allows more time for the energy transfer to take place without causing a diffuser stall.

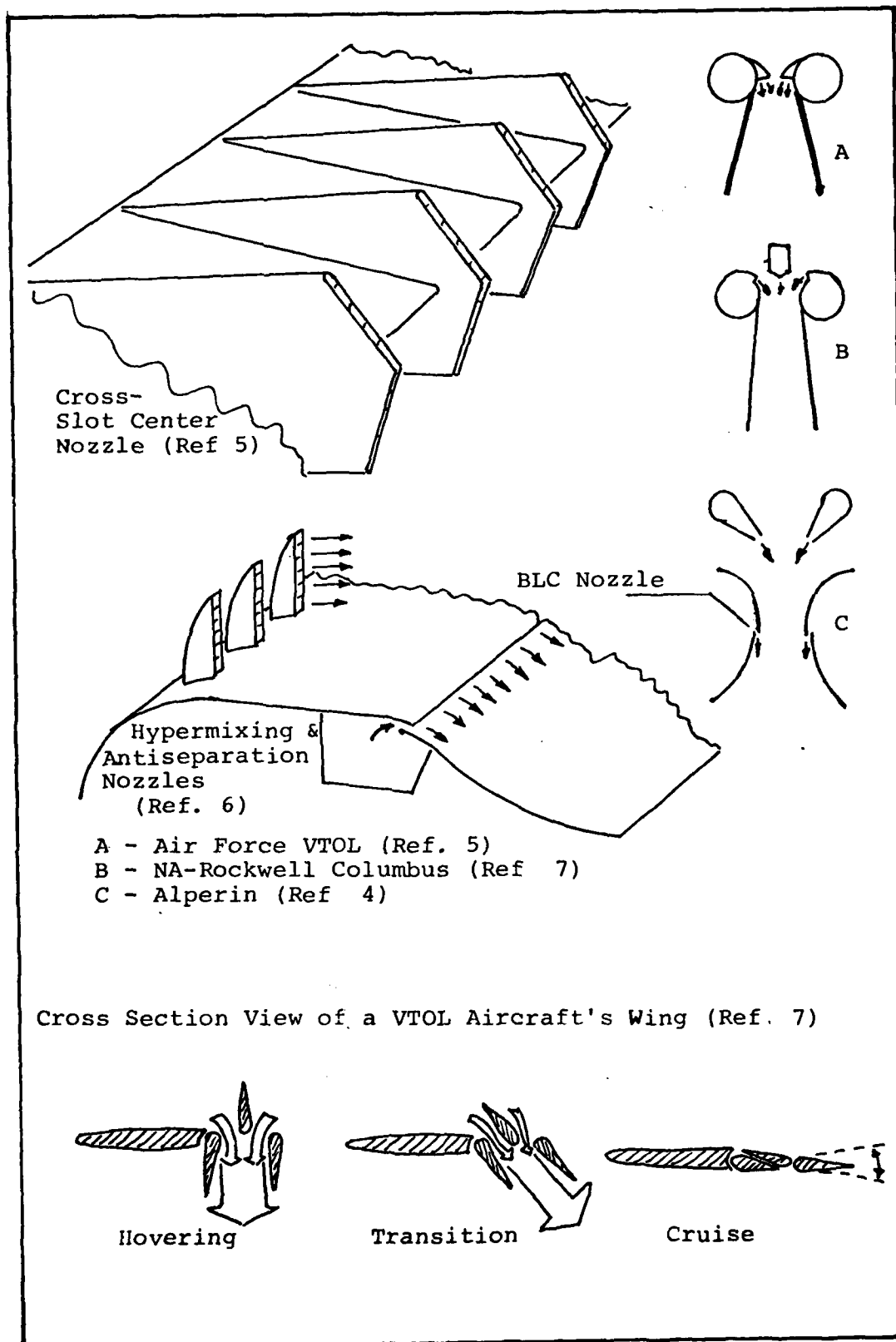


Fig. 3. Ejector Configurations

The ejectors with short diffusers and higher opening angles need BLC or antiseparation nozzles (Fig. 3). A way to incorporate an ejector into a VTOL aircraft's wing is also shown in Fig. 3.

#### Purpose and Objective

The purpose of this work was:

1. Finding the influence of the geometrical variables of a short ejector on thrust augmentation.
2. Checking the influence of the primary flow distribution on thrust augmentation.
3. Determining the influence of the variables and the flow regime on the design aspects of short ejectors.

#### Approach

In this study a short rectangular ejector was designed and fabricated. Its thrust was compared with values of thrust calculated two different ways. The comparisons were actually made by defining two different thrust augmenting ratios: The free thrust augmenting ratio and the isentropic thrust augmenting ratio. The free thrust augmenting ratio is the ratio of the ejector's measured thrust to the sum of the nozzles' measured thrust, if each of them were discharged separately to the ambient pressure. The isentropic thrust augmenting ratio is the ratio of the ejector's measured thrust to the calculated thrust of the nozzles if discharged isentropically to the ambient pressure.

In order to be able to calculate values of the free thrust augmentation, the thrust of each nozzle had to be calibrated as a function of its total pressure. The thrust of the ejector was then measured for various geometrical configurations and different primary mass flow rate distributions. The free thrust augmentation results obtained dictated the necessity of some modification (.e.g, shrouds at ejector's inlet and exit, reduced span of center nozzle, greater air supply to end-wall nozzles). The modified ejector defined as "shrouded ejector" was then tested in the same manner as the original unshrouded ejector.

Values of mass augmentation were calculated using the total mass flow at the ejectors exit and the primary flow. The total mass flow was measured by scanning the total pressure across the exit area. The primary flow was calculated using the upstream pressure in the air supply pipes and values of the pressure drop through the measuring orifices. Some design aspects were drawn when analyzing flow phenomena in conjunction with the thrust gains obtained.

## II. Apparatus

The experimental apparatus consisted of:

1. The ejector.
2. Air supply system.
3. Instrumentation.

### The Ejector

The ejector (Figs. 4, 5, and 6) had a rectangular cross section (span 6.5 in) and a variable height. It consisted of the following components:

1. Center nozzle.
2. Coanda cylinders.
3. Side walls.
4. Diffuser cylinders.
5. Diffuser.
6. End walls.
7. End-wall nozzles.
8. Inlet and exit vertical shrouds.

All the components were made of aluminum, except the end walls, which were made of plexiglass.

The center nozzle had a plane rectangular slot with a gap of 0.080 in. Total and static pressures were measured at taps located in the plenum chamber (e.g., the cylindrical section of the nozzle's housing) and at the exit, respectively. In order to maintain a uniform

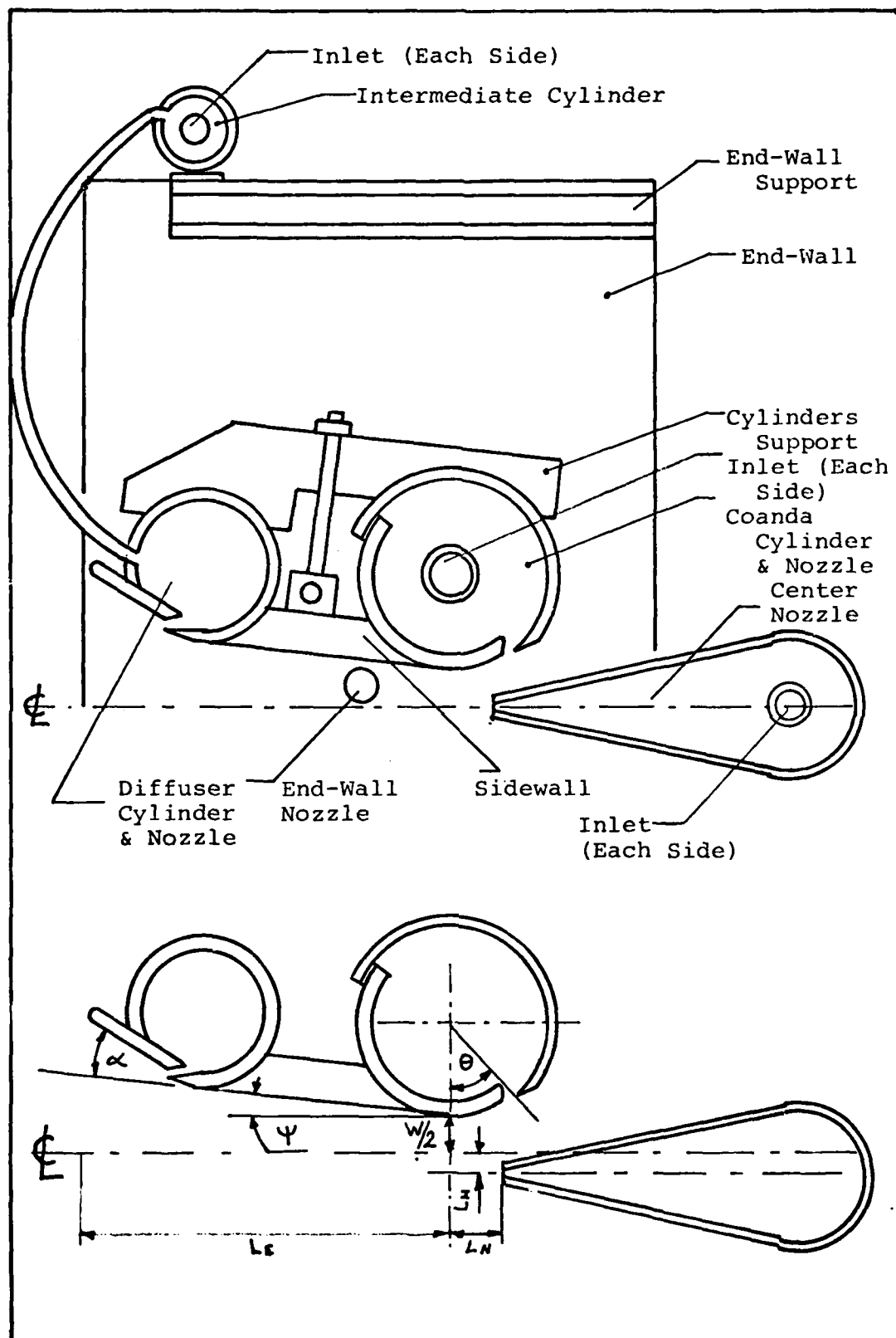


Fig. 4. Ejector Nomenclature and Variables

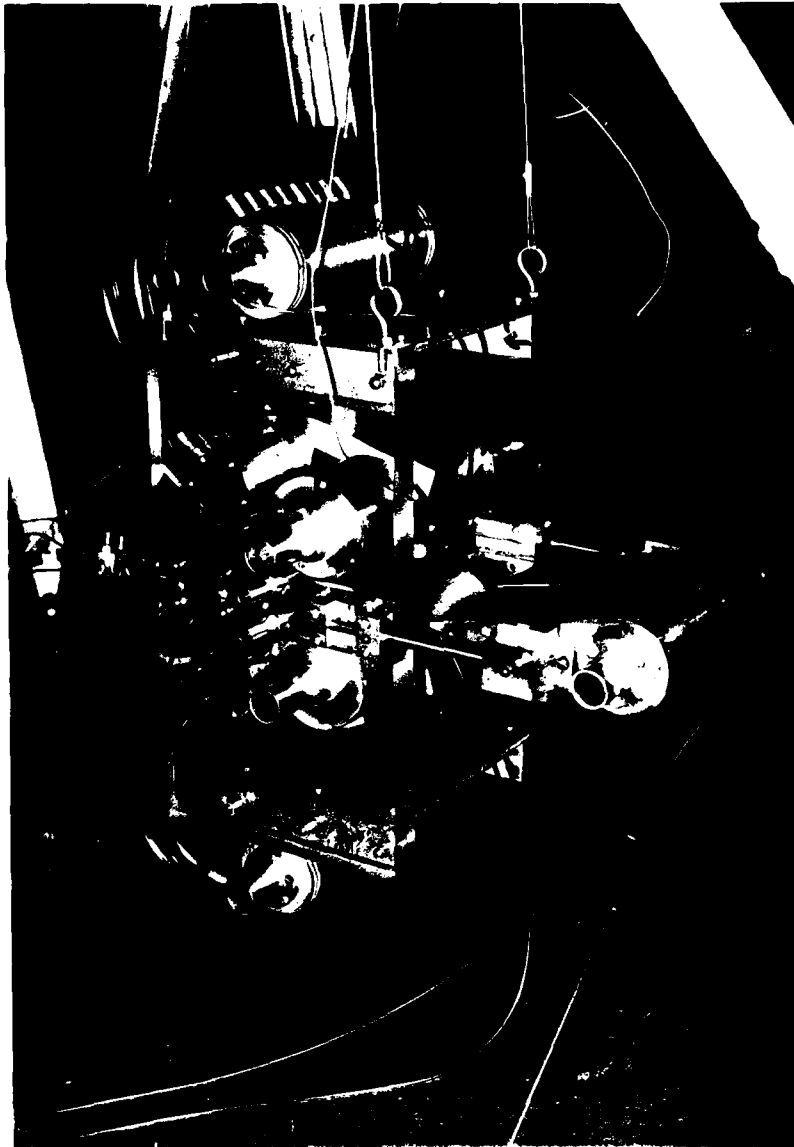


Fig. 5. Photograph of Unshrouded Ejector (Inlet View)



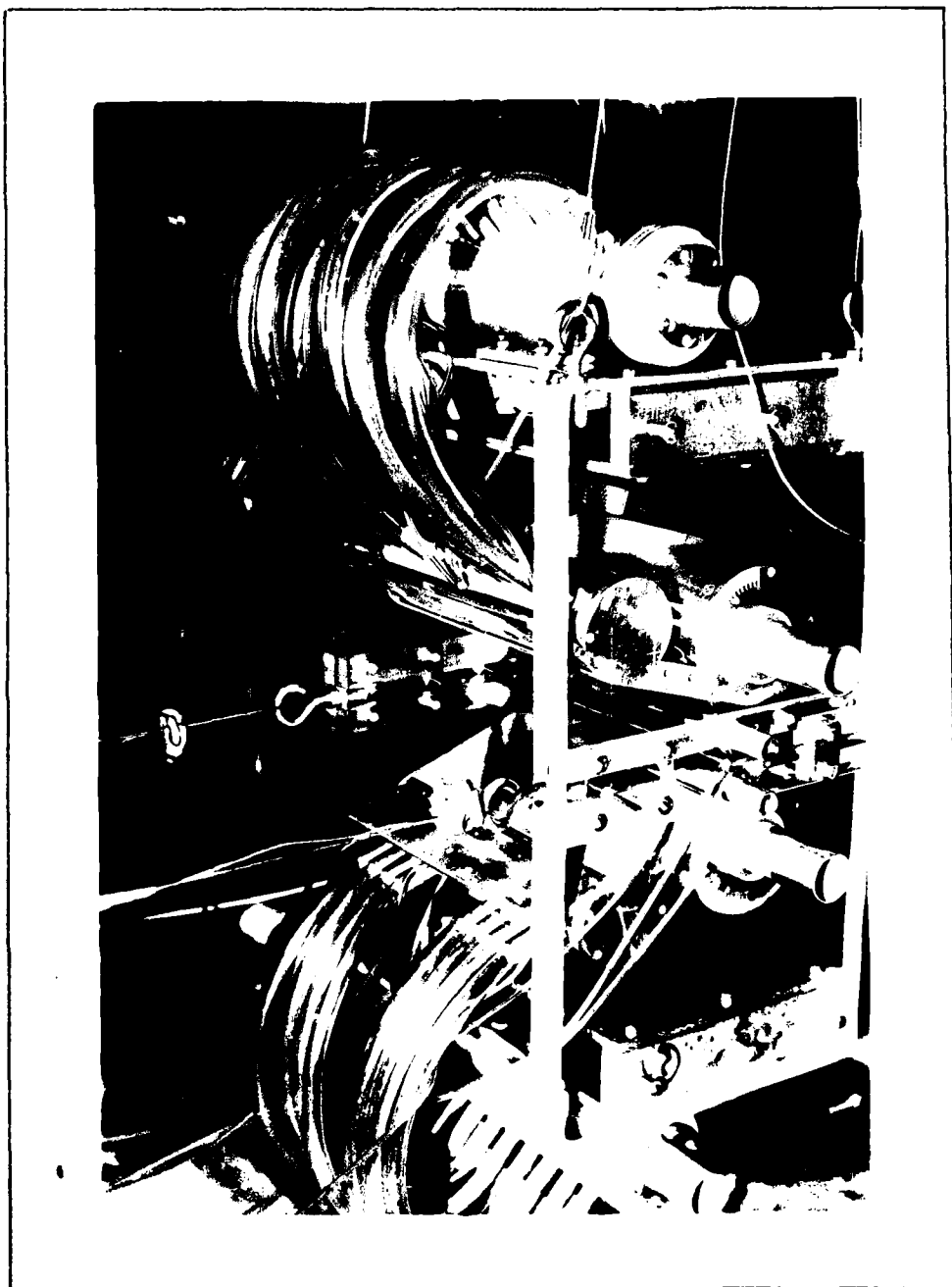


Fig. 6. Photograph of Unshrouded Ejector (Exit View)

spanwise flow, the air was introduced through a perforated pipe inserted in the nozzle's chamber. The position of the nozzle relative to the ejector could be varied by horizontal ( $0.69 \leq L_N \leq 2.65$  in) and vertical sliding. The span of the nozzle was 6.3 in. in the unshrouded ejector and 5.275 in. in the shrouded ejector configurations.

The two Coanda cylinders were located at the entrance of the ejector, and were utilized as sidewall nozzles and also served as inlet shrouds. Each had a rectangular exit slot (0.05 in.), which was strengthened by three cross pins in order to maintain constant exit area even under pressure. The cylinders could be rotated independently ( $0 \leq \theta \leq 70^\circ$ ), Fig. 4. The flow was introduced into the cylinder through a perforated pipe as in the case of the center nozzle. A total pressure tap was located in each cylinder.

The sidewalls and the fixed end walls formed the mixing chamber. The sidewalls could be adjusted to a desired opening angle ( $0 \leq \psi \leq 35^\circ$ ), Fig. 4. Three static pressure taps were located at the upstream edge of the sidewalls.

The two diffuser cylinders were located at the diffuser entrance. Each had a rectangular exit slot (0.03") which was strengthened by three cross pins like in the Coanda cylinder. A total pressure tap was located in each cylinder. The cylinder could be rotated relative to the sidewall of the mixing chamber. The flow was

introduced into the cylinder through eight inlet fittings that were attached to flexible tubes from an intermediate cylinder. This arrangement enabled the diffuser cylinder to slide along the end walls, thus allowing the opening angle of the diffuser to be varied. The diffuser cylinder could be replaced by dummy cylinders without nozzles.

The diffuser was formed by the fixed end walls and the two variable sidewalls which were attached to the diffuser cylinders. The diffuser cylinder could be rotated relative to the sidewall of the mixing chamber ( $0 \leq \alpha \leq 20$ ), Fig. 4. Three static pressure taps were located at the upstream edge of the diffuser.

The end walls were made of plexiglass. Their height was varied by installing various center inserts, thus changing the ratio of throat area to nozzle area. Three static pressure taps were located along the center inserts.

The four end-wall nozzles were located on the center inserts and their flow direction could be adjusted. Their function was to energize the thickening boundary layer on the end walls. Air was supplied to the nozzles from a branch of the diffuser manifold.

The inlet and exit shrouds (Fig. 7) were added to improve the performance of the unshrouded ejector. The top and bottom edges of the inlet shrouds were bent a little to be more compatible with the inflow direction. The exit shrouds were bent outward by 4 deg.

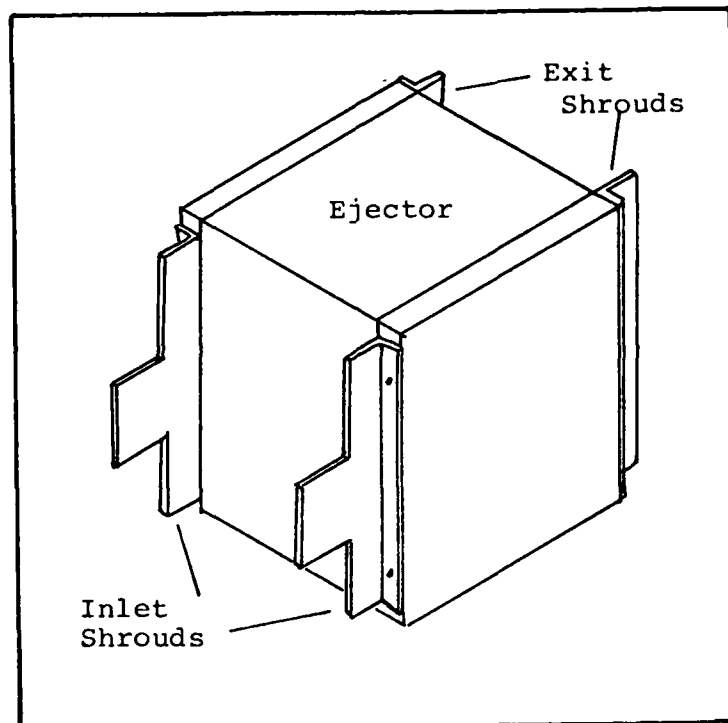


Fig. 7. Inlet and Exit Vertical Shrouds

#### Air Supply System

The primary air was supplied by two laboratory compressors. The compressed air was fed into three main pipes (Fig. 8), which were connected to flexible tubes and manifolds in the inlets of the following components:

1. Center nozzle.
2. Coanda nozzles.
3. Diffuser nozzles.
4. End-wall nozzles (branched from diffuser manifold).

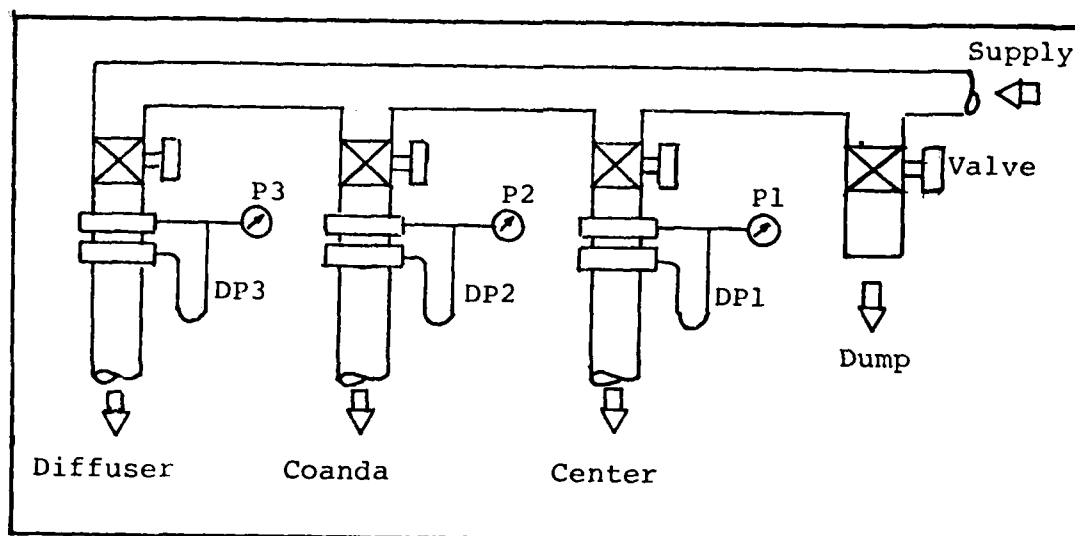


Fig. 8. Air Supply System

The flexible tubes connecting the manifolds and the ejector inlets were positioned perpendicular to the ejector in order to eliminate any influence of the increased rigidity of the pressurized tubes on the measured thrust.

The primary mass-flow rate was calculated by measuring the upstream pressure and the pressure drop through a given orifice located in each of the three main pipes. The upstream temperature was taken as the ambient temperature.

#### Instrumentation

Instrumentation requirements were concerned mainly with measurements of geometric dimensions, total and static pressure, thrust and mass flow rate.

The geometric variables  $L_N$ ,  $W$ ,  $\theta$ ,  $\psi$ ,  $\alpha$  shown in Fig. 4 were measured directly. The exit areas of the nozzles were fixed. The area and length ratios were derived from the above variables.

Total and static pressures were measured with U-tubes filled with water or mercury. Total pressures were measured at the following locations:

1. Center nozzle chamber (1).
2. Coanda cylinders (2).
3. Diffuser cylinders (2).
4. Diffuser manifold (1).
5. Scanning pitot tube (1).

Static pressures were measured at the following locations:

1. Center nozzle exit (1).
2. Upstream edge of mixing chamber sidewalls (6).
3. Upstream edge of diffuser sidewall (6).
4. Center inserts of end walls (6).

Static upstream pressure and pressure drop through measuring orifices were measured in the three supply pipes. The locations of the pressure taps are shown in Fig. 9.

The thrust of the ejector was exerted by cables, pulleys, and lever mechanisms on a strain gauge, while the ejector was hanging as a pendulum (Figs. 10 and 11). The strain gauge was a part of a Wheatstone Bridge. The exerted force disturbed the equilibrium of the bridge,

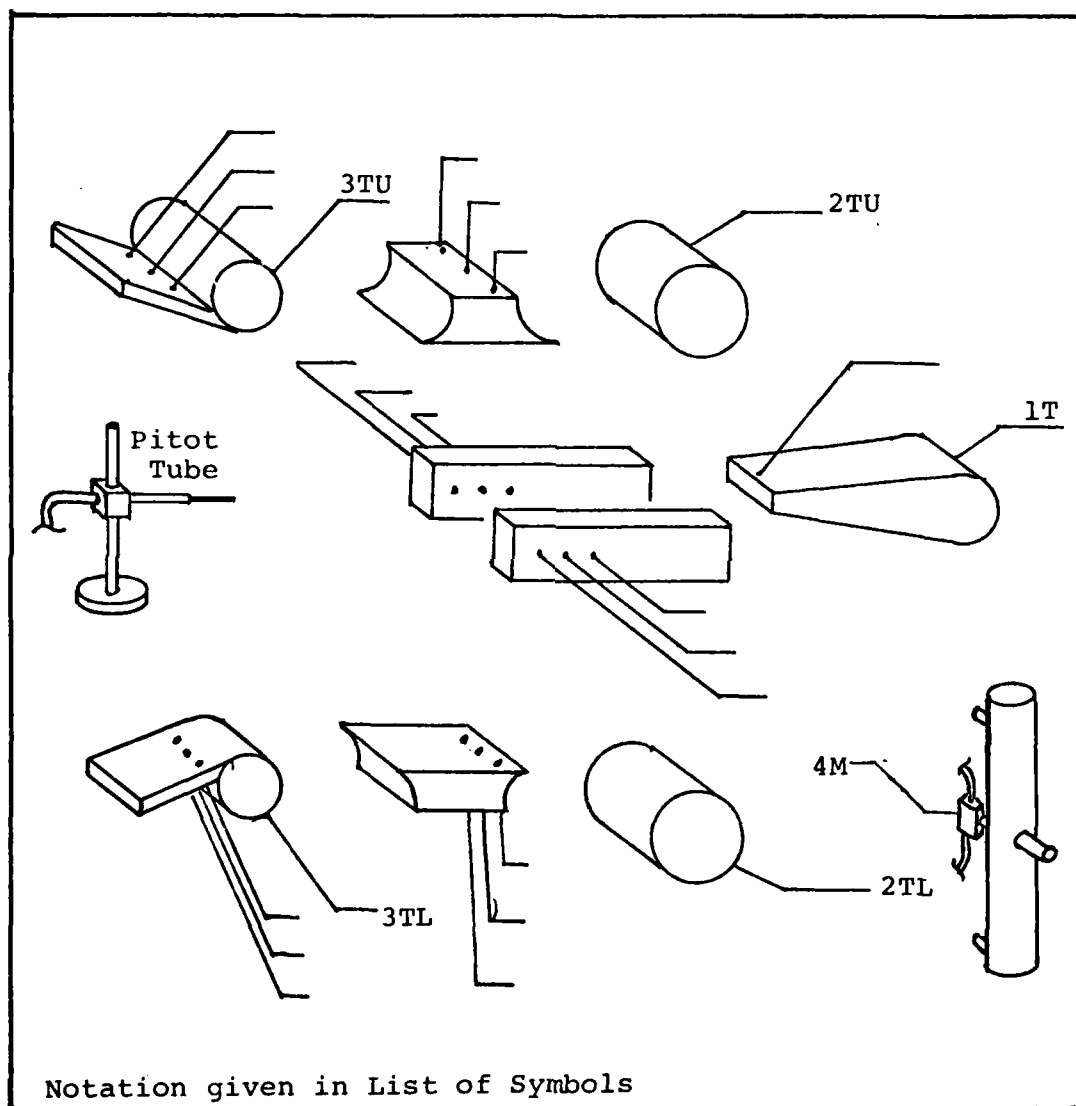


Fig. 9. Total and Static Pressure Taps

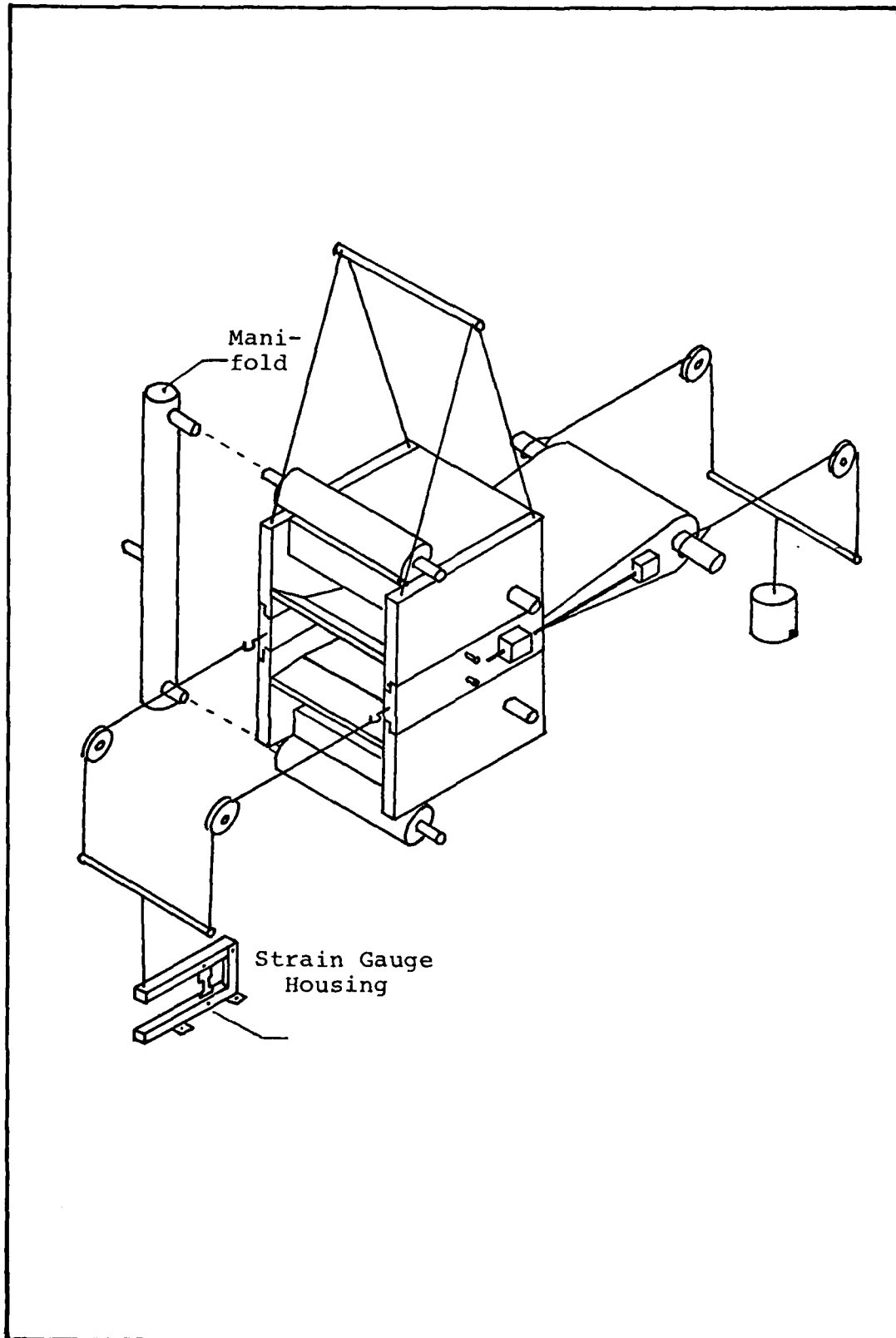


Fig. 10. Sketch of Ejector Installation



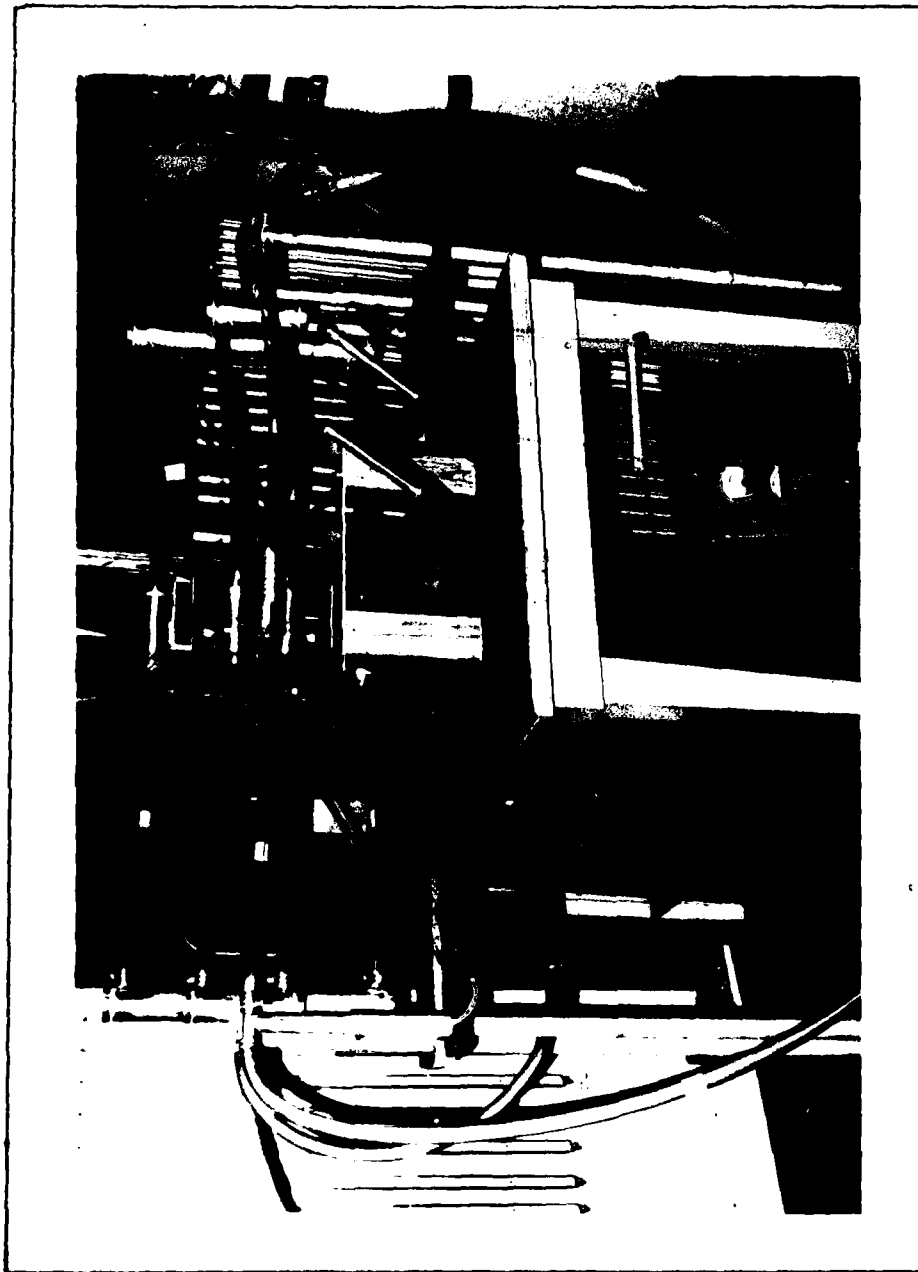


Fig. 11. Photograph of Ejector Installation

which was gained back by a variable resistor. The resistor which was built-in the strain meter was calibrated with standard weights.

Flow phenomena were traced by the behavior of a light tuft in the flow. The tuft was attached to the tip of the hand-held slender rod.

### III. Experimental Procedures and Data Reduction

The experiments were run in two phases:

1. Thrust calibrations were done separately for each of the following nozzles:
  - a. The center nozzle (full and reduced span).
  - b. The Coanda nozzles.
  - c. The diffuser nozzles (including the end-wall nozzles.
  - d. The end-wall nozzles by themselves.
2. Thrust measurement of various geometric configurations and different primary flow distributions. Initially, runs were made on the unshrouded ejector with a wide range of variables, in pursuit of the best flow/geometry configuration. Then runs were made on the shrouded ejector that were focused on the promising configuration found through the results and analysis of the initial runs. During a few tests total mass flow measurements were made in both ejectors (unshrouded, shrouded).

#### Thrust Equation

The equation for calculating the isentropic thrust of a nozzle which is discharged to ambient pressure is:

$$F_i = 7A_e P_a [(P_t/P_a)^{0.2857} - 1] \quad (1)$$

This equation is obtained by substituting the equation for velocity of an isentropic compressible flow (equation 2) into the equation of momentum flux (equation 3). Using  $\gamma = 1.4$ .

$$v_e = \sqrt{\frac{2\gamma}{\gamma-1} \frac{P_a}{\rho_a} \left[ \left( \frac{P_t}{P_a} \right)^{\frac{\gamma-1}{\gamma}} - 1 \right]} \quad (2)$$

$$F_i = \rho_a A_e v_e^2 \quad (3)$$

Note that the isentropic thrust of a nozzle is independent of temperature.

#### Thrust Calibration of the Nozzles

In order to calculate the free thrust augmentation  $\phi_f$ , the thrust of each nozzle was measured separately (i.e., not assembled in the ejector) when the pressure in the nozzle plenum was discharged to ambient pressure. The thrust obtained was defined as the free thrust of the nozzle. The isentropic thrust was calculated by substituting the measured absolute total pressure and the absolute ambient pressure in Eq. (1).

The Coanda and diffuser nozzle were tested with the sidewall in place; otherwise the flow would surround the cylinder due to the Coanda effect, and the thrust could

not be measured. The calibration of the diffuser nozzle was done with the end-wall nozzles in place.

#### Data Reduction for Nozzle Thrust

To account for losses in the isentropic thrust, loss coefficients were calculated as follows: Eq. (1) was rearranged to Eq. (4).

$$\ln \left( \frac{F_i}{7A_e P_a} \right) + 1 = 0.2857 \ln \left( \frac{P_t}{P_a} \right) \quad (4)$$

For isentropic flow without losses, the RHS equals the LHS. The outcome using the measured free thrust  $F_f$  for various total pressures instead of the isentropic thrust  $F_i$  is a relation of the form

$$\ln \left( \frac{F_f}{7A_e P_a} + 1 \right) = K_1 * 0.2857 \ln \left( \frac{P_t}{P_a} \right) + K_2 \quad (5)$$

where  $K_1$  and  $K_2$  are loss coefficients that were found by linear regression of the data obtained for each nozzle, and are given in Table I.

The free thrust of the nozzle is:

$$F_f = 7A_e P_a \left[ e^{K_2} * \left( \frac{P_t}{P_a} \right)^{0.2857 * K_1} - 1 \right] \quad (6)$$

TABLE I  
NOZZLE'S LOSS COEFFICIENTS

Nozzle	$K_1$	$K_2$
Upper Coanda	0.709604	0.007539
Lower Coanda	0.645095	0.0025
Upper Diffuser	0.64963	0.00196
Lower Diffuser	0.38934	0.001885
End Wall	0.221	0.00313

#### Primary Flow Calculations

The primary flow calculations were based on the ASME procedure described in Ref 3. Two variables were considered in these calculations. The upstream pressure in the air supply pipe and the pressure drop through a measuring orifice. Detailed explanations of the calculation method are given in Appendix A.

#### Total and Secondary Flow Calculations

The total outflow at the ejector's exit was calculated using the continuity equation

$$\dot{m} = \rho AV \quad (7)$$

where  $\rho$  was taken as the ambient density, which is justified for subsonic flow. The exit area was divided

into rectangular subareas to account for the nonuniform velocity across the exit, and the velocity for each subarea was taken as the average of the velocities in its four corners.

The velocities at the corners of the subareas were measured with a pitot tube. The sum of the flows through the subareas was the total flow. Detailed explanations of the program used for total flow calculations are given in Appendix B.

The secondary flow is the difference between the total flow and the primary flow.

#### IV. Results and Analysis

The results and analysis discussed in this chapter are divided into four categories:

1. Calibration results of the nozzles.
2. General flow phenomena.
3. Thrust augmentation results.
4. Ejector's exit flow results.

##### Calibration Results of the Nozzles

###### Center Nozzle

The center nozzle free thrust was within 1 percent of the isentropic thrust for both spans (original and reduced). This means that a rectangular straight nozzle with a converging plenum can be assumed for design purposes having no losses. The reason for no-losses in such a nozzle is that the converging geometry toward the exit, generates small velocities near the walls of the nozzle housing while the maximum velocity is at the exit.

###### Coanda and Diffuser Nozzles

Fig. 12 shows the free thrust [Eq. (6)] for each of the Coanda and diffuser nozzles and their isentropic thrust [Eq. (1)].

Fig. 13 gives the ratio of the isentropic thrust to the free thrust of the nozzles. Note that the thrust



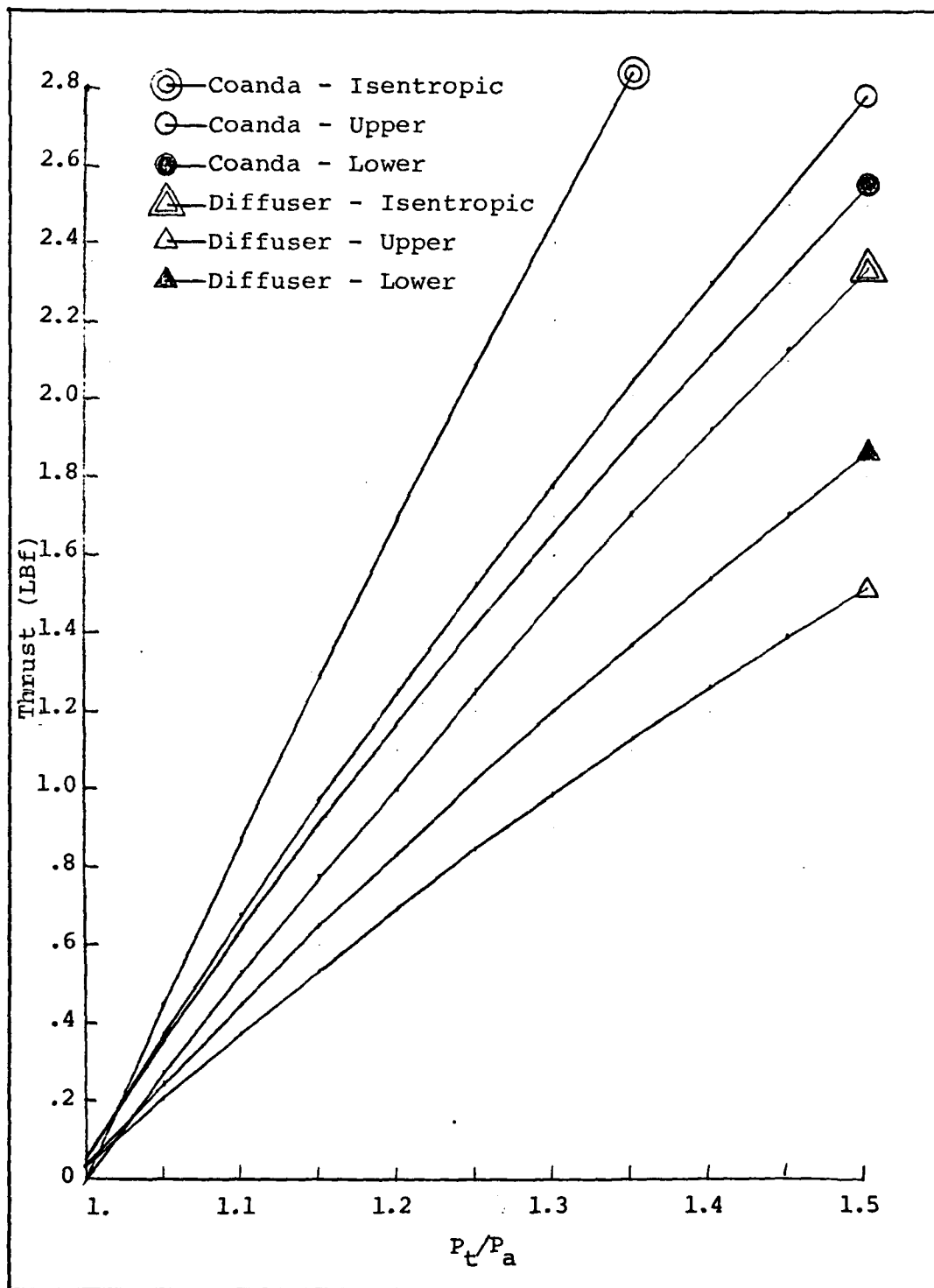


Fig. 12. Coanda and Diffuser Nozzle Thrust vs. Pressure Ratio

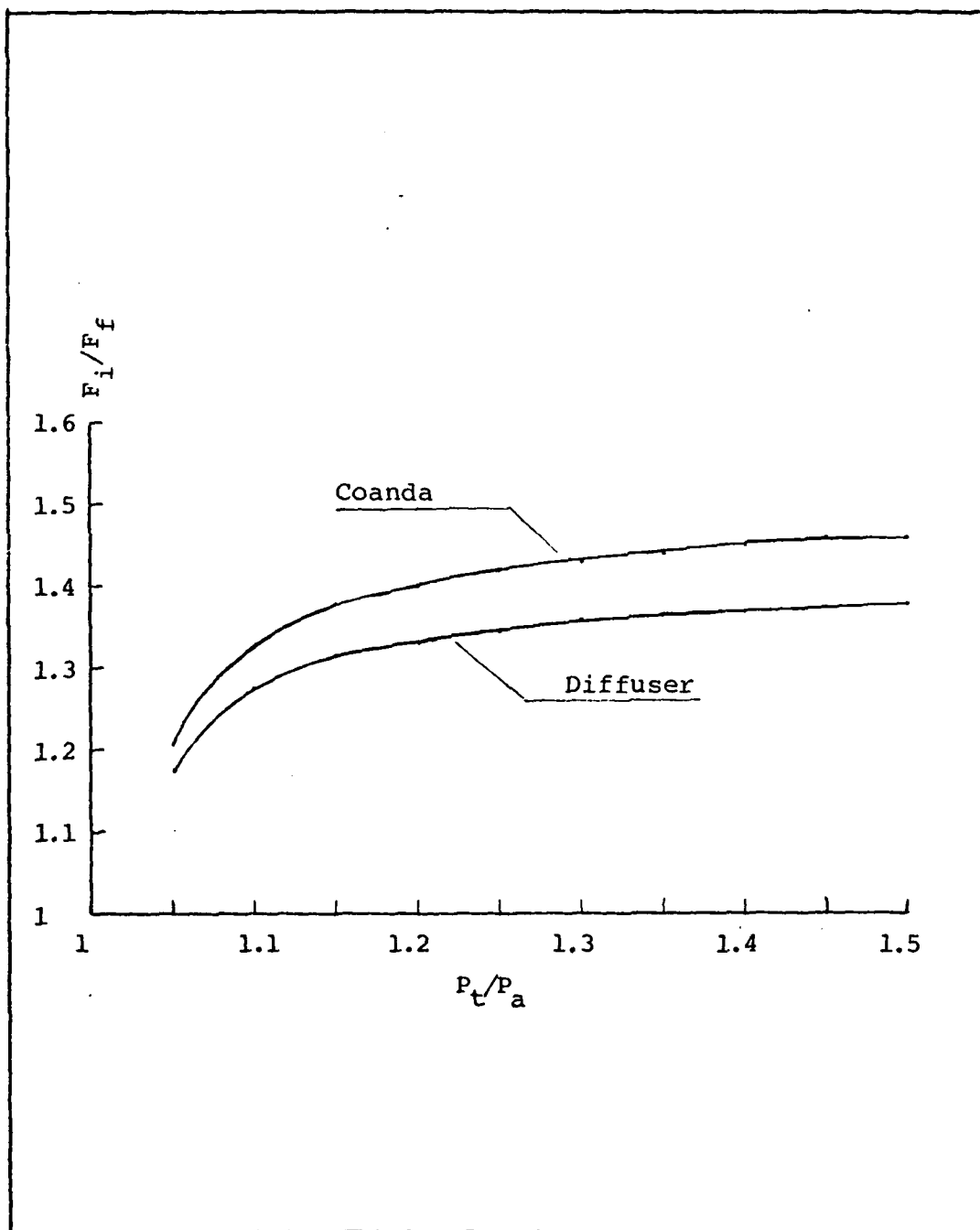


Fig. 13. Isentropic and Measured Coanda and Diffuser Nozzle Thrust Ratio vs. Pressure Ratio

of the diffuser nozzle includes also the thrust of the two adjacent end-wall nozzles.

Fig. 14 shows the same variables for the end-wall nozzles by themselves.

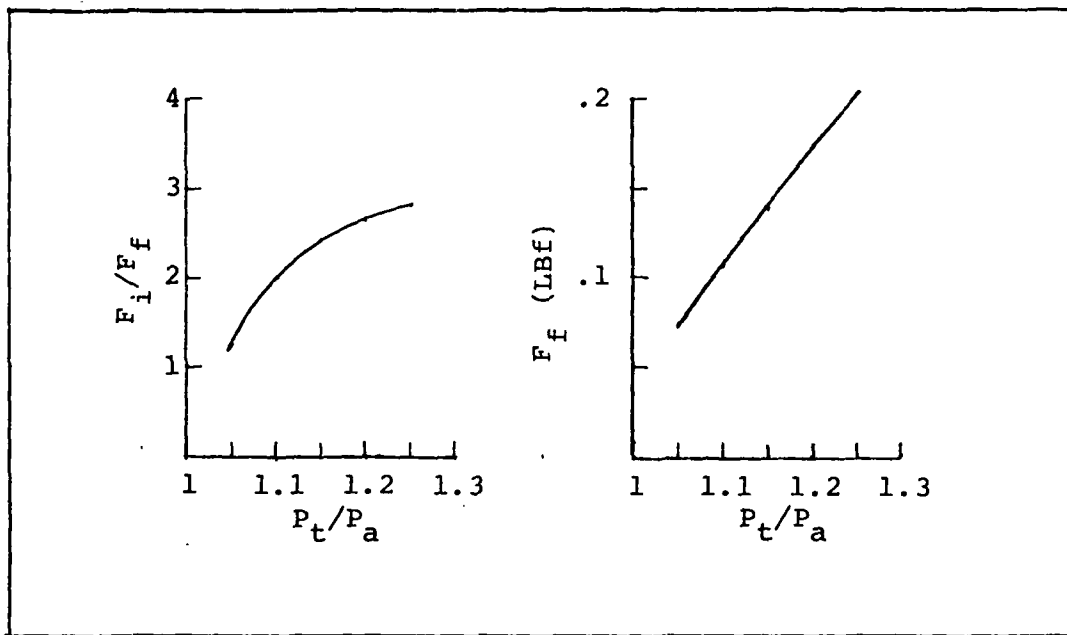


Fig. 14. Thrust and Thrust Ratio vs. Pressure Ratio for End-Wall Nozzles

From the graphs it can be seen that:

1. The isentropic thrust of each nozzle is reduced when the air jet is blown tangential to a wall. This is shown in Figs. 12 to 14 where the free thrust is less than the isentropic thrust.
2. The thrust ratio  $F_i/F_f$  of the diffuser nozzle was better ( $F_i/F_f$  lower, Fig. 13) than that of the Coanda nozzle, because of the shorter sidewall's length its flow

had to travel. Without the inclusion of the two adjacent end-wall nozzles, the thrust ratio would have been even better.

3. The difference in thrust between nozzles of the same type is probably due to measurement errors. Locations of total pressure taps and asymmetries in fabrication.

4. The thrust loss of the end-wall nozzles is high, due to three reasons:

a. The outflow has a fan-like pattern, and it is not directed entirely parallel to the flow direction.

b. The jets are directed tangential to the end walls.

c. The total pressure is measured in the manifold and not near the exit.

#### General Flow Phenomena

The flow phenomena are described for both the unshrouded and shrouded ejector. The shrouded ejector configuration is a modified version of the original ejector that was unshrouded. The ejector modifications were done following the results and flow analysis of the unshrouded ejector. They included not only vertical shrouds (Fig. 7), but also a reduction of 15 percent to the center nozzle's span and blocking off the air supply to the diffuser nozzles, such that the air supply to the end-wall nozzles could be controlled directly.

The flow phenomena were traced by a light tuft attached to the tip of a slender hand-held rod. The direction, fluctuation and swirl of the tuft provided a visual indication of the flow, including vortices, turbulence and stall regions.

#### Flow Phenomena in Unshrouded Ejector

The relatively poor performance of the unshrouded ejector was due to:

1. Vortex flow at the inlet, shown in Fig. 15, that distorted the uniform velocity profile of the nozzle's exit jet. Although the vortices increased the

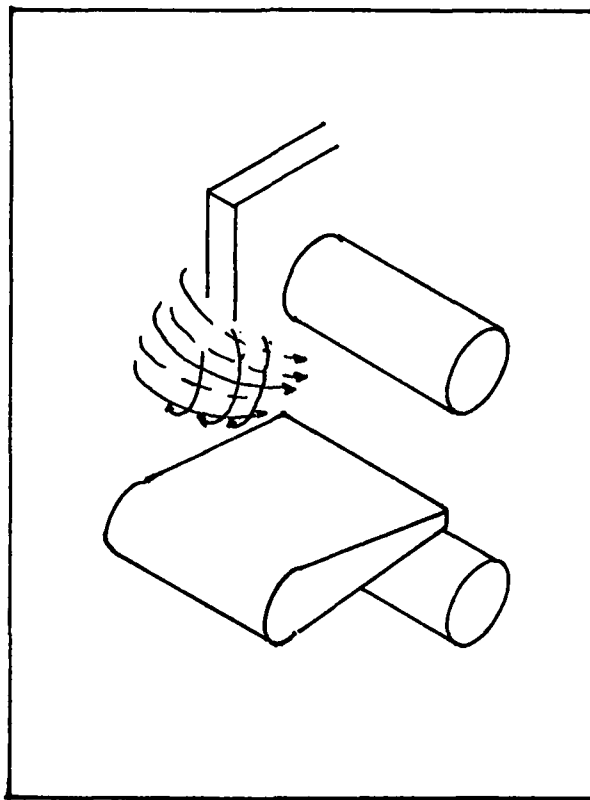


Fig. 15. Vortex Flow at Ejector Inlet

turbulent flow in the ejector and contributed to the flow mixing, they were--according to the results--very dissipative.

2. Local stall regions at the two ends of the horizontal center line of the ejector exit. The stall regions are shown in Fig. 16.

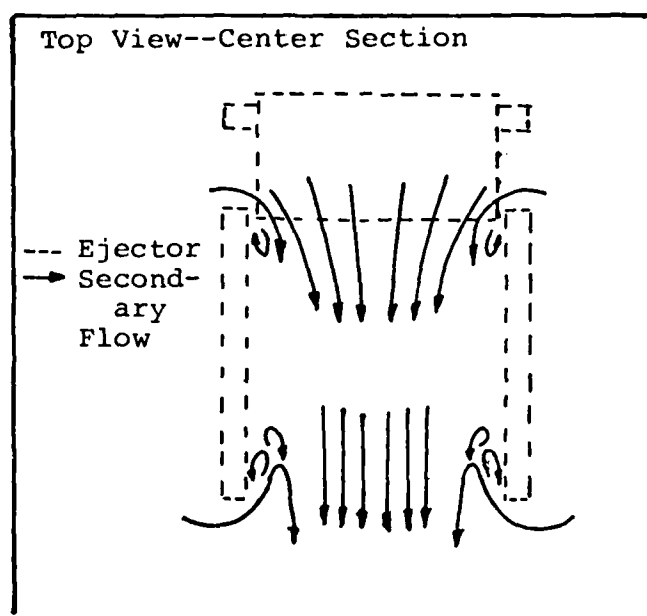


Fig. 16. Local Stall Region in the Ejector

#### Flow Phenomena in Shrouded Ejector

The modification mentioned earlier improved significantly the flow characteristics in the ejector by eliminating or reducing the vortices in the inlet and the stall regions at the exit. Thus, the flow became more two dimensional and smoother, although some turbulent spots could still be detected.

The vertical inlet shrouds caused a reduction in the flow at the inlet of the ejector. This caused a reverse flow (Fig. 17) generated by the low pressure region at the inlet. This reverse flow along the ejector's sides reduced the ejector's thrust.

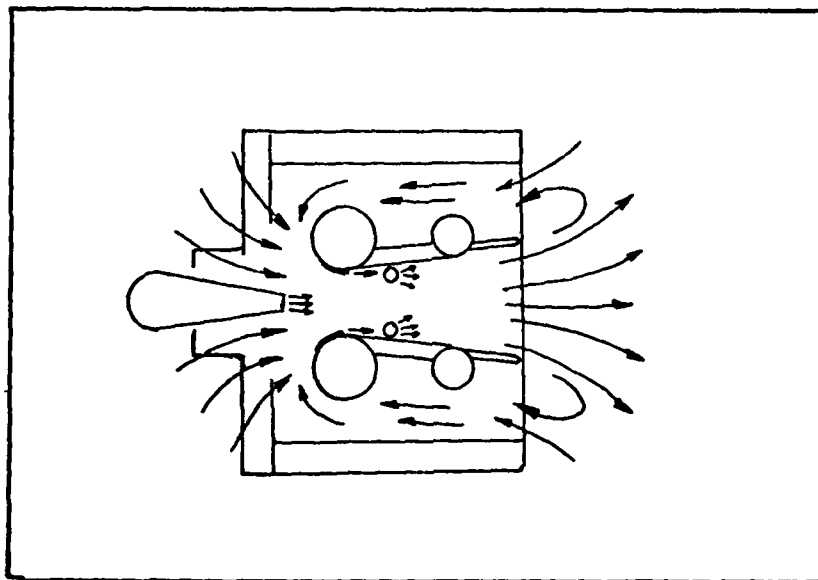


Fig. 17. Reverse Flow

Another general flow phenomenon found (in both the shrouded and the unshrouded ejectors) was a bi-stable stall (Fig. 18) when the center nozzle jet was on by itself. The stall occurred even with parallel diffuser sidewalls, if the throat width and the center nozzle location were such that the diverging jet could not touch both sidewalls simultaneously. This phenomenon is due to the Coanda effect.

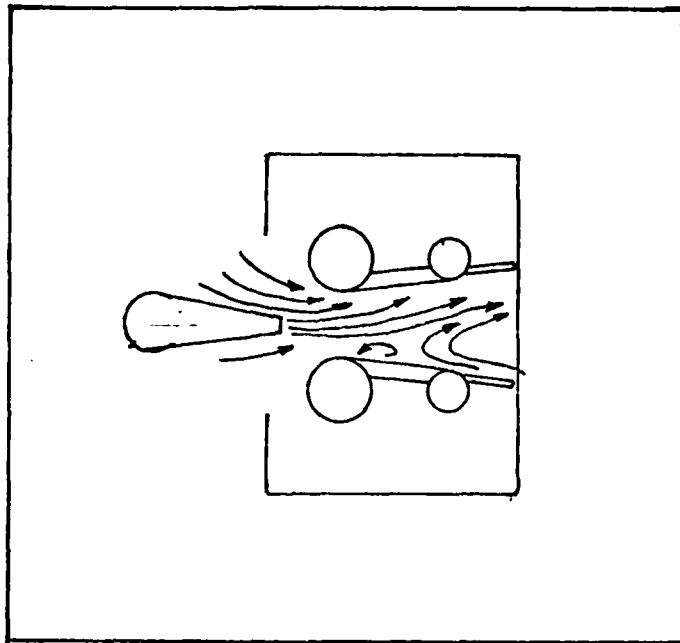


Fig. 18. Center Nozzle Jet's Stall

#### Thrust Augmentation Results

Thrust augmentation results are given for both the unshrouded and shrouded ejector. In both ejectors only three throat widths were investigated ( $w=1.56, 2.24, 2.9$  in.). Although the geometrical variables ( $\psi, \theta, \alpha, L_N$ ) and the flow distribution could be changed continuously, some distinct values were chosen to limit the amount of runs. Three values of  $L_N$  (inner most, outer most, and intermediate) and three values of  $\theta$  (0, maximum possible, and intermediate) were selected. The maximum values of  $\theta$  depended on  $\psi$  and are given in Table II. Four values of  $\psi$  (0, 10, 15, and 20 degs) were chosen.  $\psi$  was the most sensitive geometric variable, since a small change in the



variable caused a significant change in thrust. The selection of the flow distribution among the nozzles was such that in each case one nozzle was the dominant primary flow nozzle. The selected values are given in Tables III, IV, and V. For clarity all the values are designated and these designations are used in the presentation of the results.

TABLE II  
 $\theta_{\max}$  VALUES

$\psi$ , deg	$\theta_{\max}$ , deg
0	70
10	65
15	60
20	55

TABLE III  
 $L_N/W$  VALUES

Designation	W (in)	$L_N$ (in)	$L_N/W$
Unshrouded			
$L_N/W1$	1.56	0.69	0.44
$L_N/W2$		1.72	1.10
$L_N/W3$		2.75	1.76
$L_N/W4$	2.24	0.69	0.31
$L_N/W5$		1.72	0.77
$L_N/W6$		2.75	1.23
$L_N/W7$	2.91	2.75	1.06
Shrouded			
$L_N/W8$	2.24	1.5	1.49
$L_N/W9$		2.65	0.85
$L_N/W10$	2.91	2.65	1.1

TABLE IV

## AR VALUES

Designation	Throat Area (in <sup>2</sup> )	Center and Coanda Nozzles Area (in <sup>2</sup> )	AR
Unshrouded			
AR1	10.15	1.14	8.8
AR2	14.54	1.14	12.7
AR3	18.93	1.14	16.6
Shrouded			
AR4	10.15	1.06	9.6
AR5	14.54	1.06	13.7
AR6	18.93	1.06	17.8

TABLE V  
DISTRIBUTION OF PRIMARY MASS FLOW VALUES

Designations	Percent of Primary Flow Through Nozzles			
	Center	Coanda	Diffuser*	End-Wall
Unshrouded				
MR1	50	26	24	N/A**
MR2	21	52	27	N/A
MR3	36	28	36	N/A
Shrouded				
MR4	54	41	N/A	5
MR5	34	62	N/A	4
MR6	36	64	N/A	0

\*Includes four end-wall nozzles.

\*\*Not applicable.

Results for Unshrouded Ejector  
(Figs. 19 through 27)

1. The first feature that is dominant in all the curves is that the best performance was obtained wherever the Coanda nozzles were providing the main primary flow (MR2).

2. The best thrust performance obtained with MR2 occurred when  $\psi=10$  deg and

a.  $\theta = 30$  or  $60$  deg for AR1.

b.  $\theta = 60$  deg for AR2.

Thus, there was a tendency for the optimum  $\theta$  to increase with increase in AR. It will be shown later for the shrouded ejector that  $\theta$  optimum should be in the neighborhood of  $60$  deg.

3. There is a clearly expressed decrease in performance going from  $\psi=10$  to  $20$  deg in all curves. This decrease is due to regions of local stalls (discussed earlier) that are enlarged by higher diffuser angles. The end-wall nozzles were not capable of preventing these stalls because the lack of compressed air allotted to them by the diffuser nozzles.

4. The thrust performance when the diffuser nozzles were providing the main primary flow (MR3), was in some cases relatively poor (Figs. 23, 24 and 25). The only configuration that  $\phi_f$  was less than one was obtained in MR3 (Fig. 21).

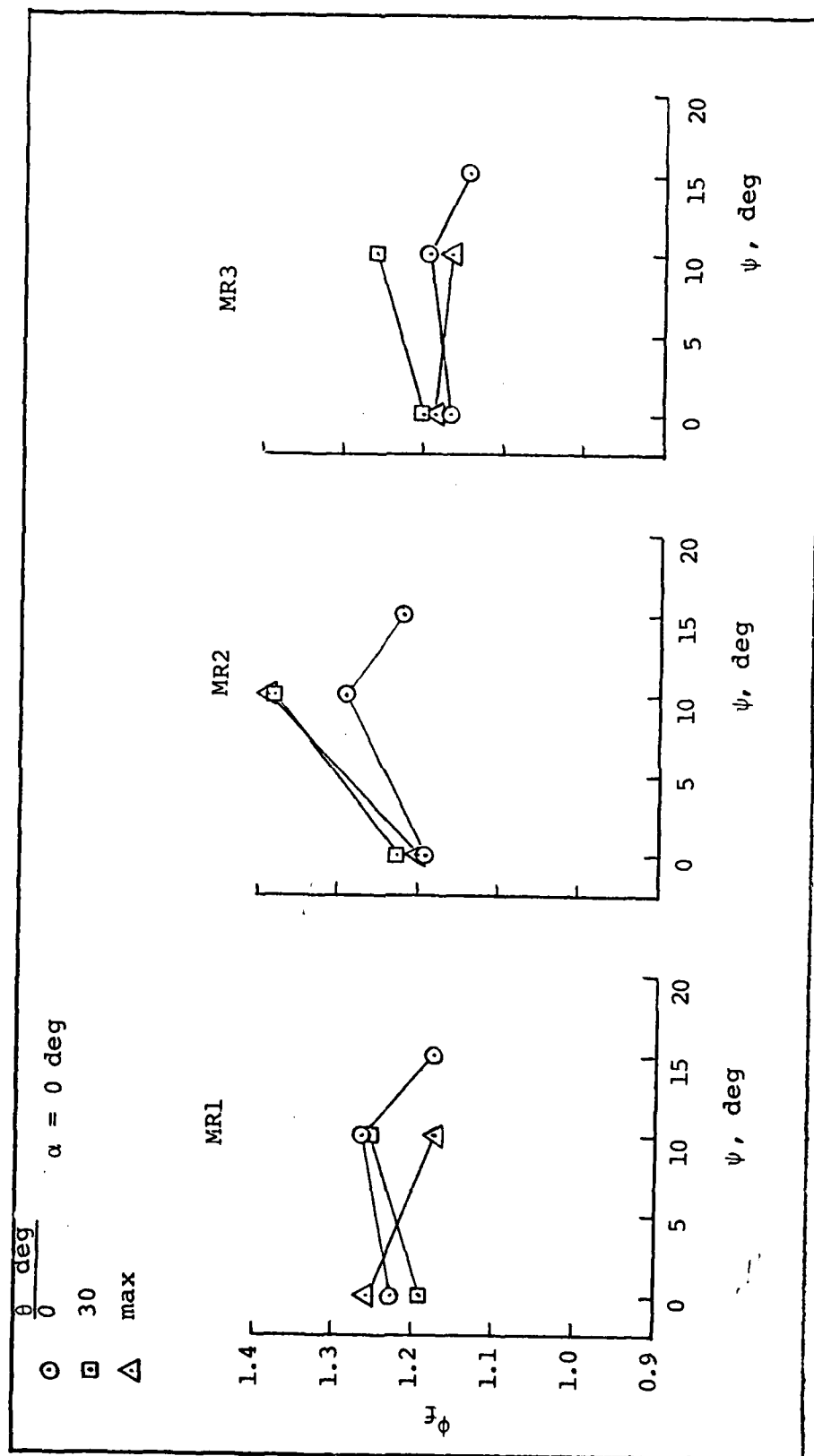


Fig. 19.  $\phi_f$  for AR1 and  $L_N/W1$  (Unshrouded)

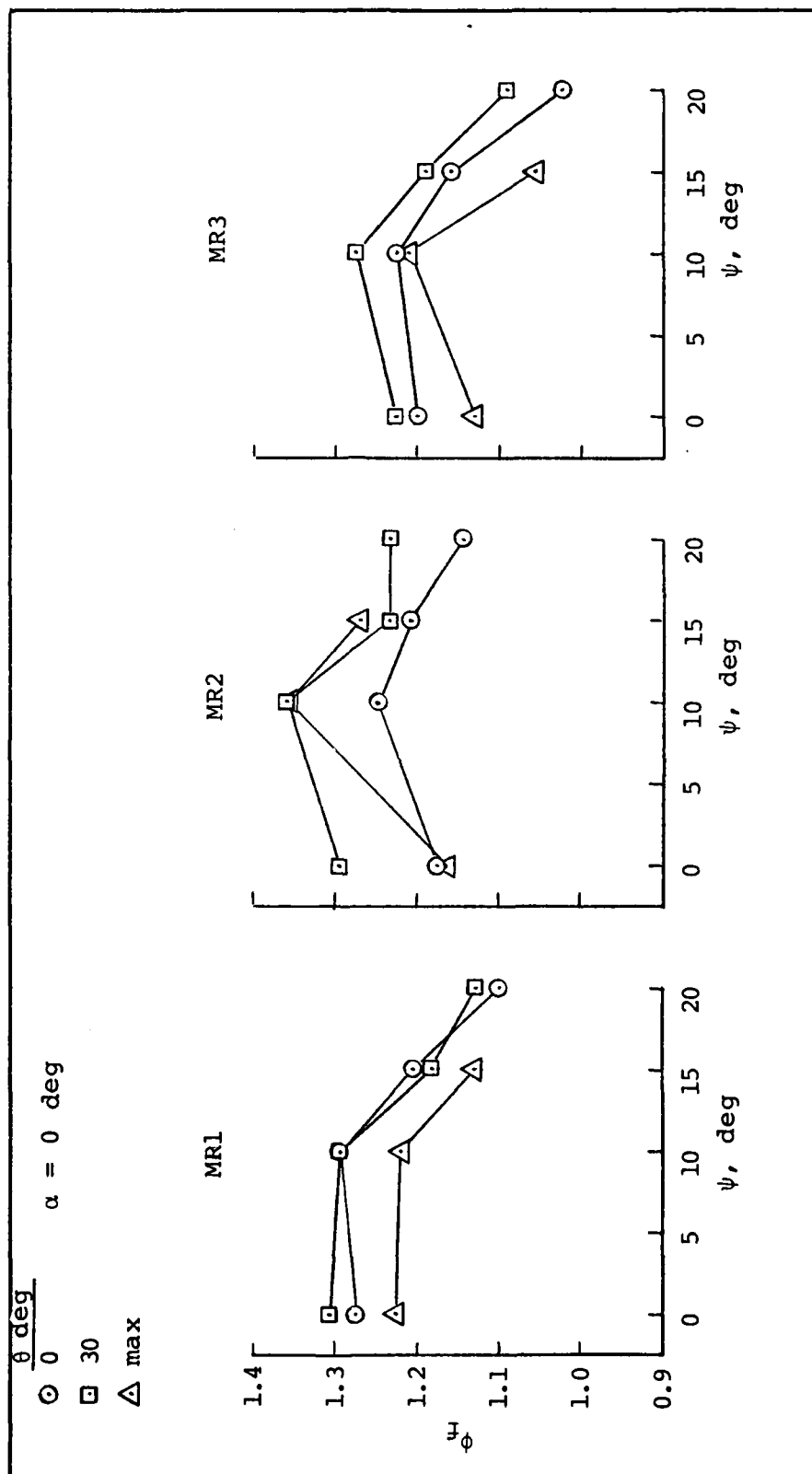


Fig. 20.  $\phi_f$  for AR1 and  $L_N/W2$  (Unshrouded)

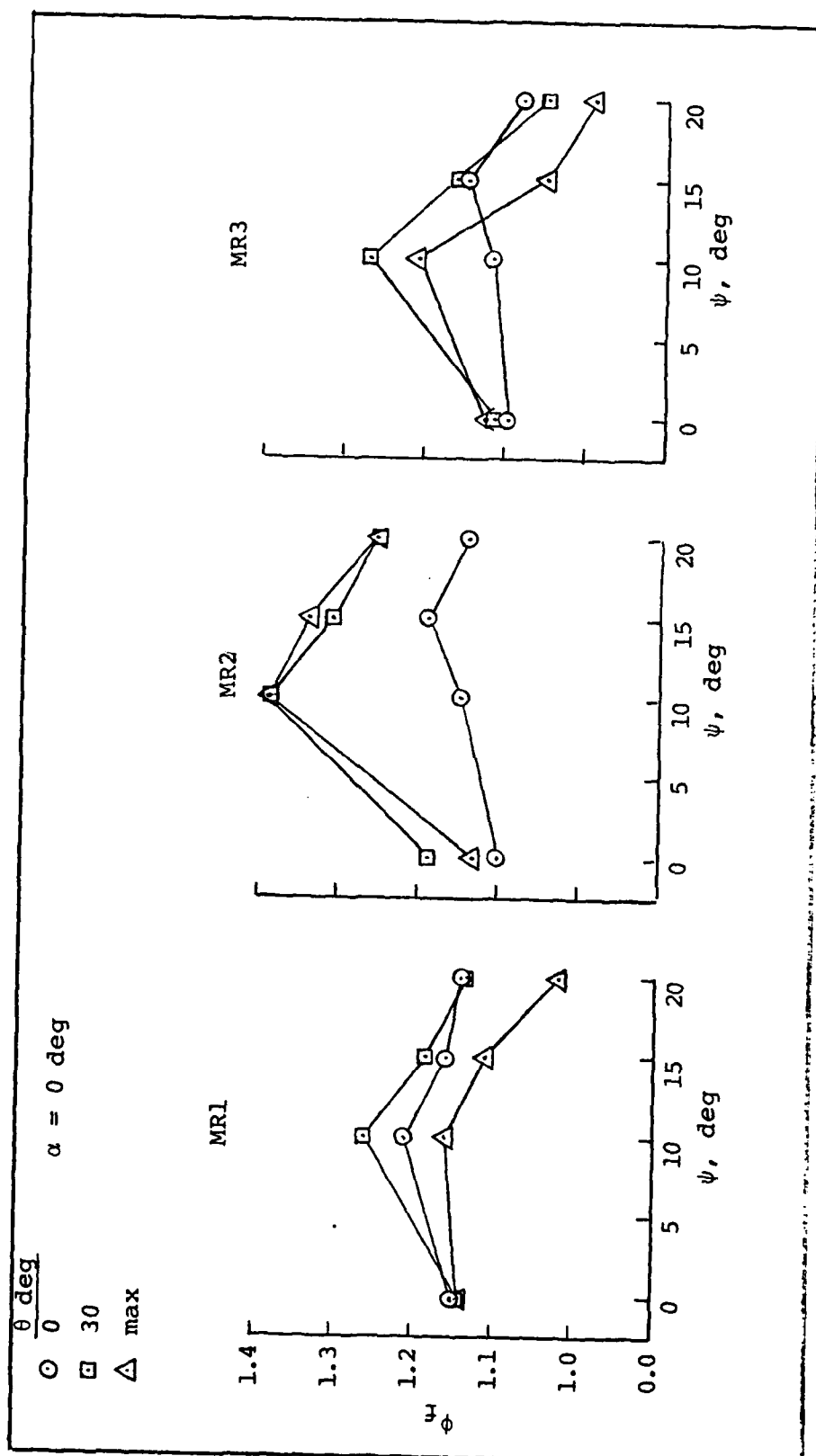


Fig. 21.  $\phi_f$  for AR1 and  $L_N/W3$  (Unshrouded)



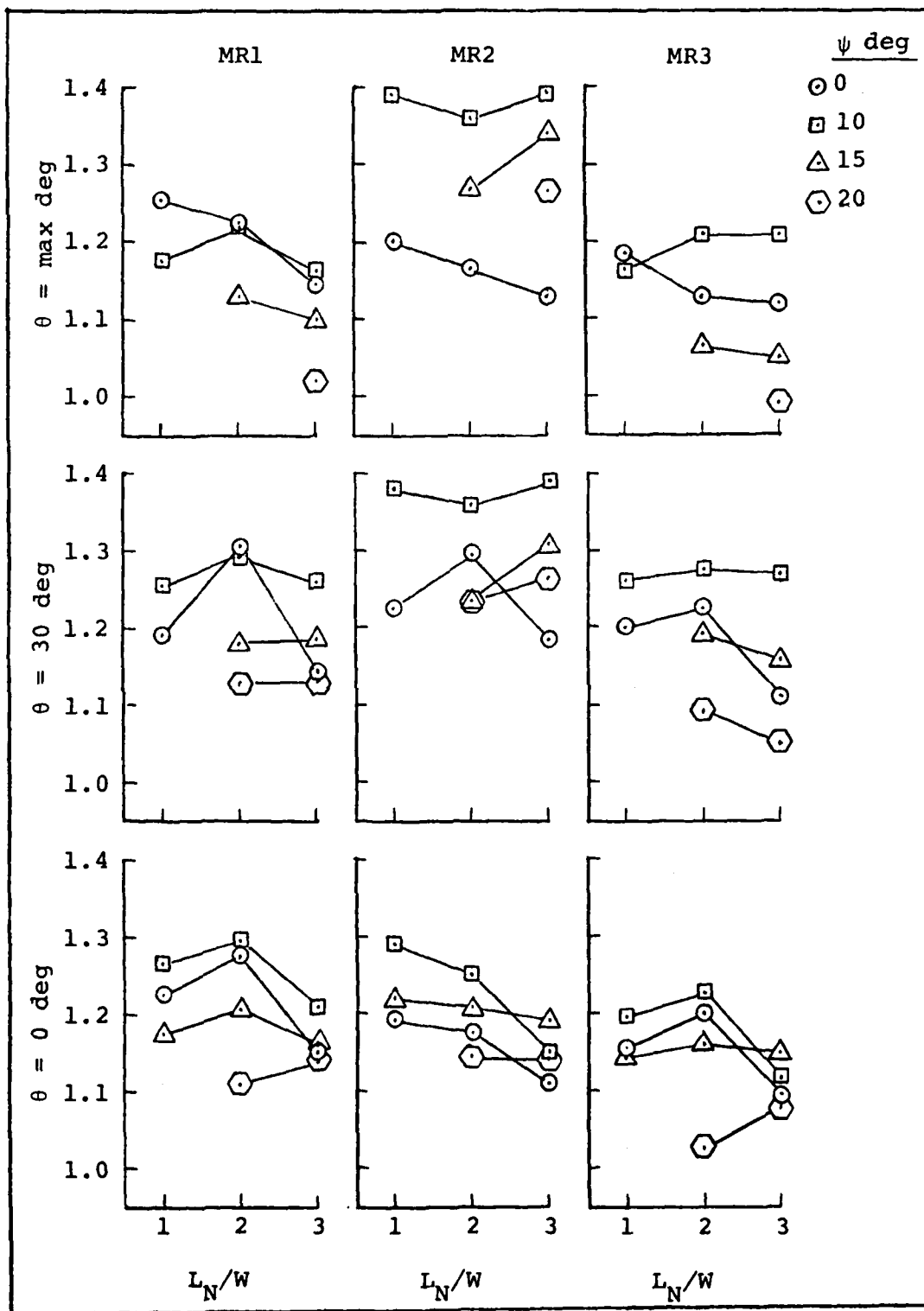


Fig. 22.  $\phi_f$  vs.  $L_N/W$  for AR1 (Unshrouded)

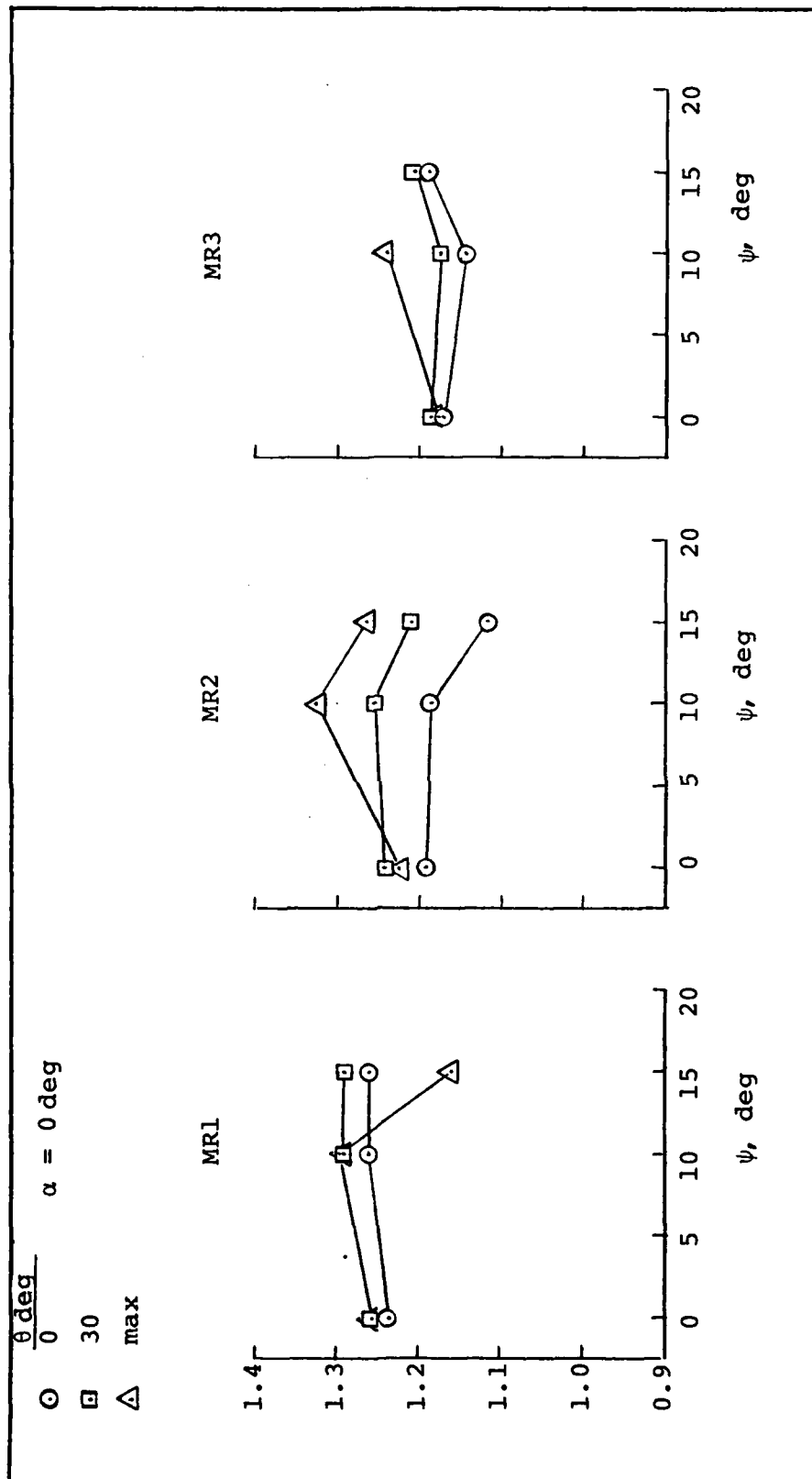


Fig. 23.  $\phi_f$  for AR2 and  $L_N/W4$  (Unshrouded)

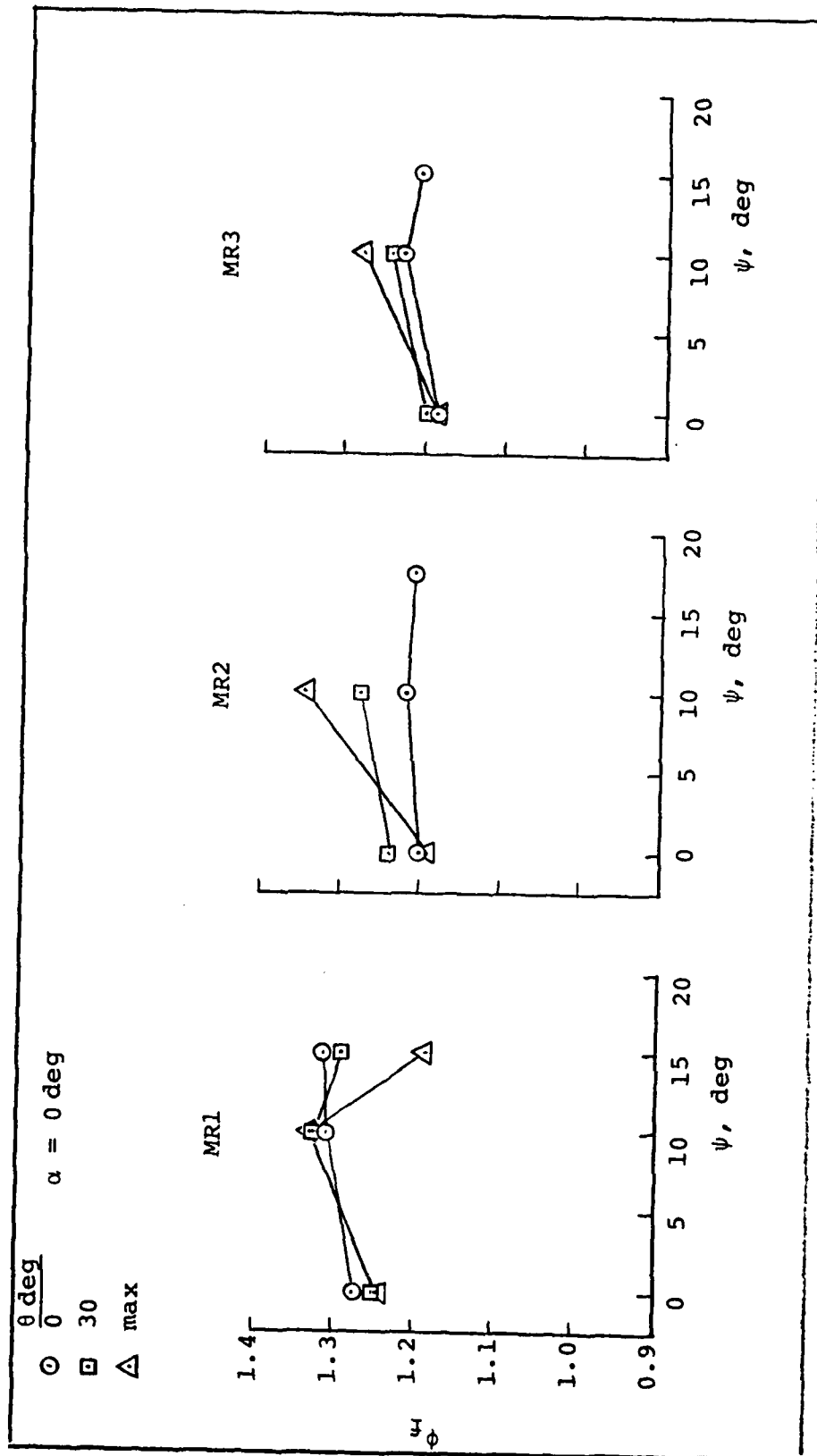


Fig. 24.  $\phi_f$  for AR2 and  $L_N/W5$  (Unshrouded)

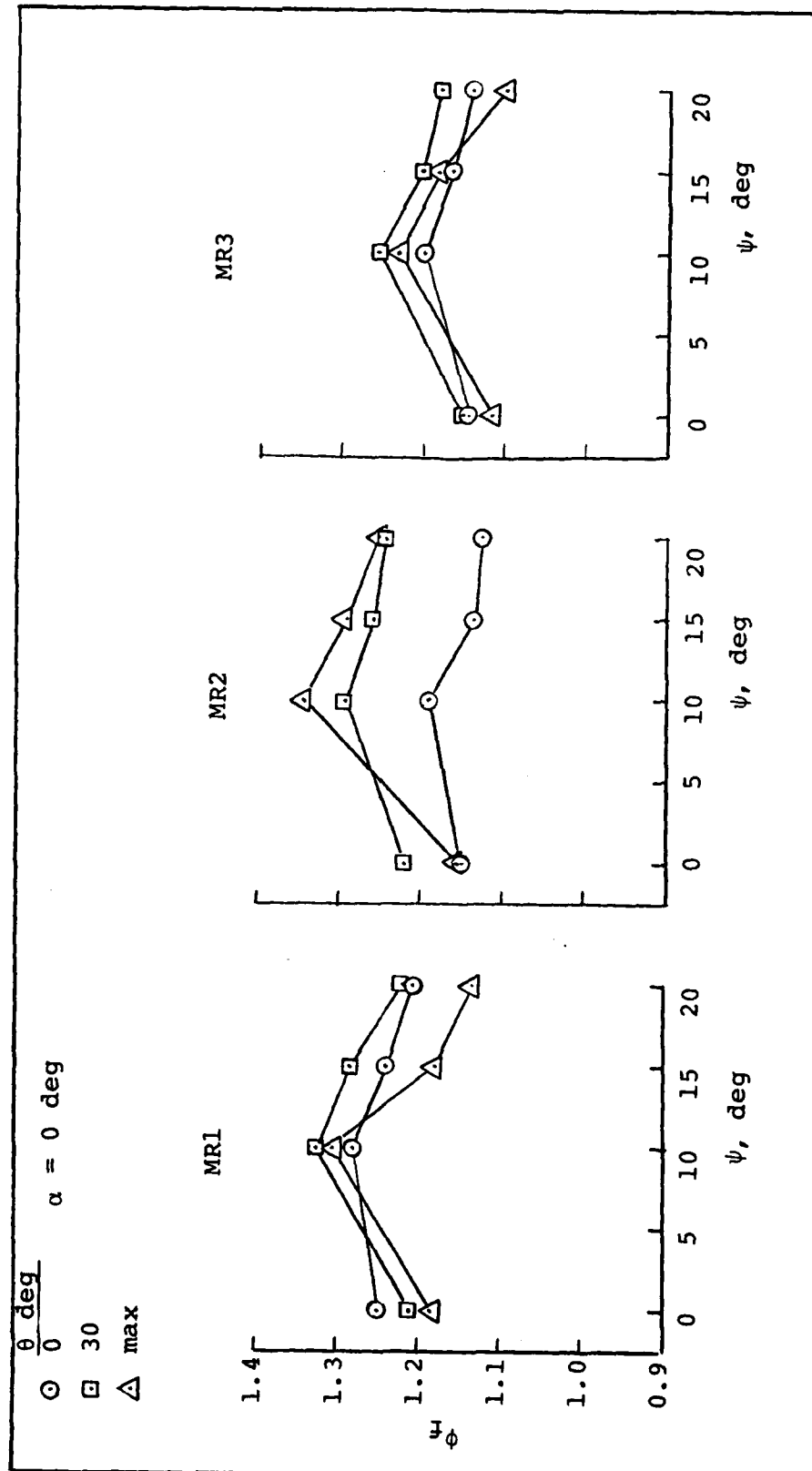


Fig. 25.  $\phi_f$  for AR2 and  $I_N/W6$  (Unshrouded)

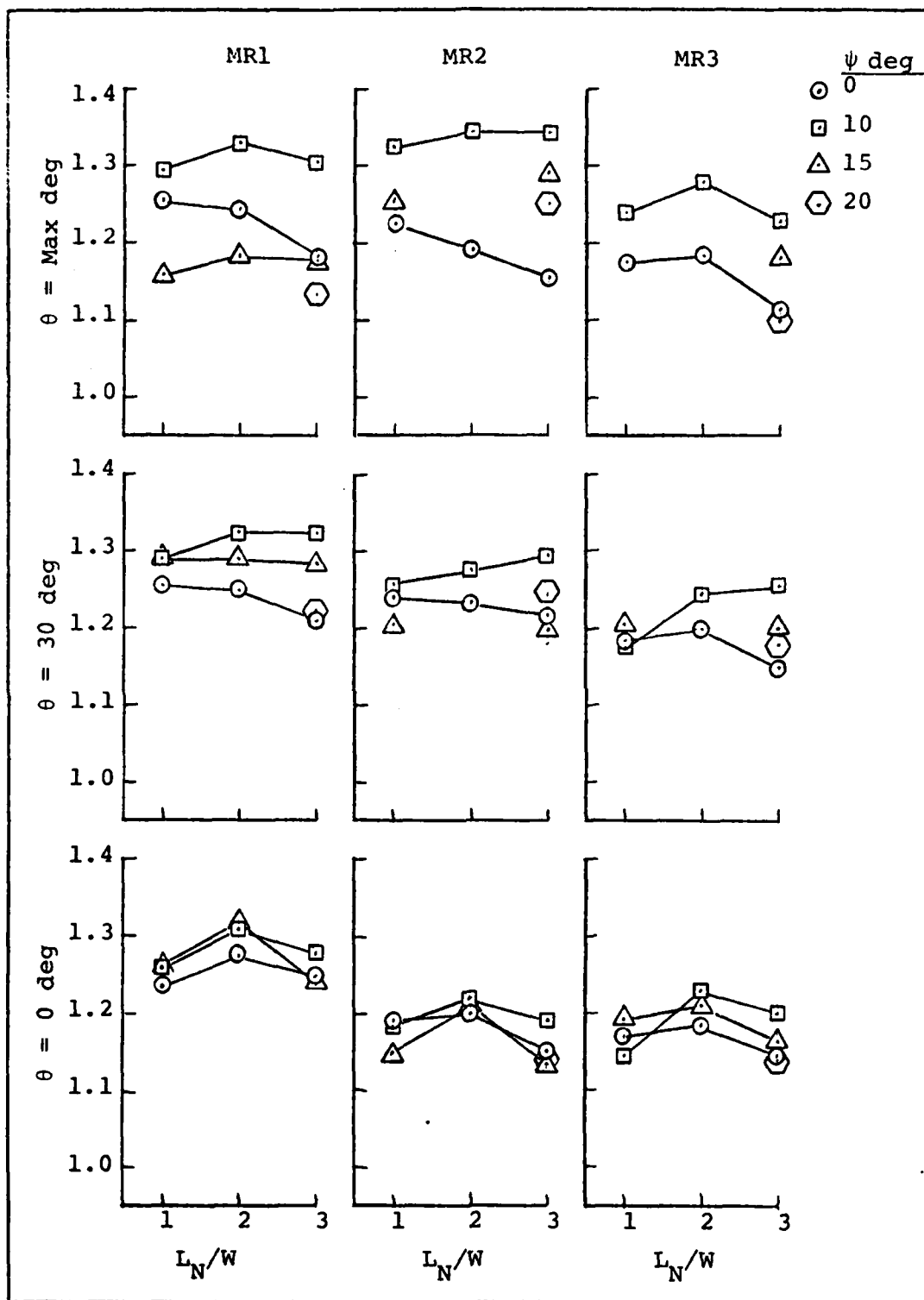


Fig. 26.  $\phi_f$  vs.  $L_N/W$  for AR2 (Unshrouded)

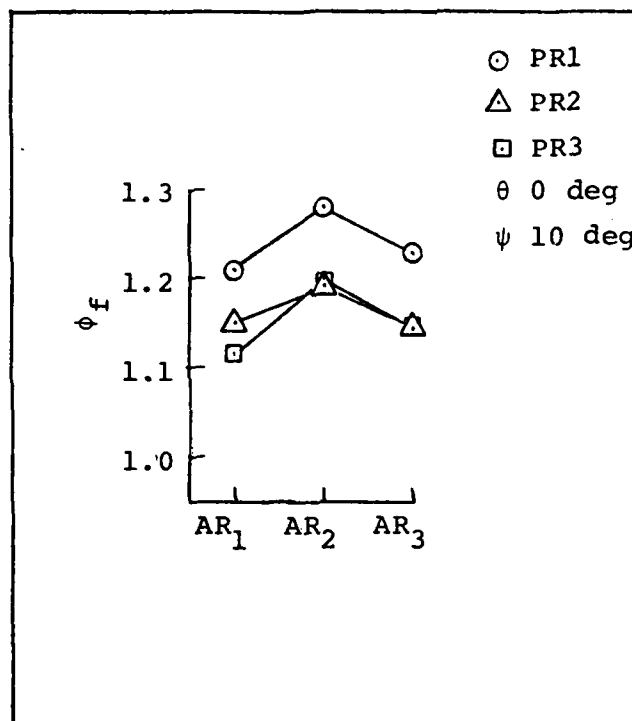


Fig. 27.  $\phi_f$  vs. AR for  $L_N = 2.5$  in (Unshrouded)

5. Performance was less for  $\theta=0$  deg for all MR2 in comparison to  $\theta=30$  and  $60$  degrees because the entrainment capability of the Coanda nozzles was not utilized (Figs. 19, 20, 21, 23, 24, and 25).

6. Coanda flow at the maximum  $\theta$  angles for MR1 and MR3 was most wasteful because high  $\theta$  angles caused stronger vortex flow into the inlet and did not reduce the local stall regions at the exit. This led to a reduction in the thrust that could have been obtained by the center nozzle or the diffuser nozzle as the main primary nozzles (Figs. 19, 20, 21, and 25).

7. The influences of  $L_N/W$  on  $\phi_f$  seems to have sometimes a contradictory behavior. For instance, comparing for the case MR2 and  $\psi=10$  deg in Figs. 22 and 26 at different AR shows that no significant change occurs in  $\phi_f$  due to location of the center nozzle, except for  $\theta=0$  deg and the lower AR where there is a significant increase in thrust when the center nozzle is closer to the diffuser. The reason is that in at lower AR when  $\theta=0$  deg the flow from the Coanda nozzles was able to decrease the local stalls at the exist, thus decreasing the losses of the direct thrust of the center nozzle. The nearer the jet of the center nozzle was to the exit, the less losses it suffered and thus the increased thrust.

8. An overview of the results from the unshrouded ejector shows that results cannot always be predicted

from other results, aside from the common features that were already mentioned. Examples of the unpredicted behavior are:

a.  $\phi_f$  for the cases of MR1 and MR3 in Figs. 20, 21, 23, 24, and 25 is increasing for an increase in  $\psi$  from 0 to 10 deg, while it is decreasing for the same change in  $\psi$  in Fig. 19.

b.  $\phi_f$  for MR3 is maximum at  $\psi=10$  deg for all cases except for  $L_N/W4$ ,  $\theta=30$  and 60 deg (Fig. 23) where it becomes a minimum at that  $\psi$ .

Such a behavior is due mainly to two reasons:

a. Turbulency, vortices and local stalls in the flow. These undesired phenomena can influence differently the thrust for the same change in a given variable, if a second variable is different, e.g.,  $\phi_f$  for  $\psi=0$  (MR2,  $\theta=30$  and 60 deg) increases when sliding the center nozzle from  $L_N/W3$  to  $L_N/W2$  while decreasing for the same change in  $L_N/W$  when  $\psi=10$  and 15 deg (Fig. 22).

b. Inaccuracy in measurement. The pressure readings off the U-tubes were taken visually one at a time, while the pressure supply was not always steady enough. Besides, the resolution of visual reading of mercury is not good enough for small differences in pressures.

9. In general, it can be said that short ejectors are less tolerant to shifts from the optimum design.



### Results for Shrouded Ejector

Following the results and analysis of the unshrouded ejector some modifications were made in the ejector as mentioned earlier. The performance of the shrouded ejector is shown in Figs. 28 and 29.

The main features of these graphs are:

1. The shrouded ejector had a performance better than that of the unshrouded version. Fig. 28 shows a comparison (the white and black circles) of  $\phi_f$  for the same configuration shrouded and unshrouded.
2. The results with the shrouded ejector appear to be more predictable than those from the unshrouded ejector.
3. As in the unshrouded ejector the best performance occurs when the main primary flow is provided by the Coanda nozzles (MR5).
4. The optimum  $\theta$  angle is 60 degrees.
5. The importance of the end-wall nozzle is clearly seen in Figs. 28 and 29 where the flow distribution for MR5 is almost the same as for MR6, but the thrust gain decreased by an average of 25 percent without the flow from the end-wall nozzles.
6. The isentropic augmenting thrust ratio is less than the free thrust augmenting ratio (Fig. 28). This reduction is greater for MR5 where the Coanda nozzles are the main primary nozzles than for MR4 where the center

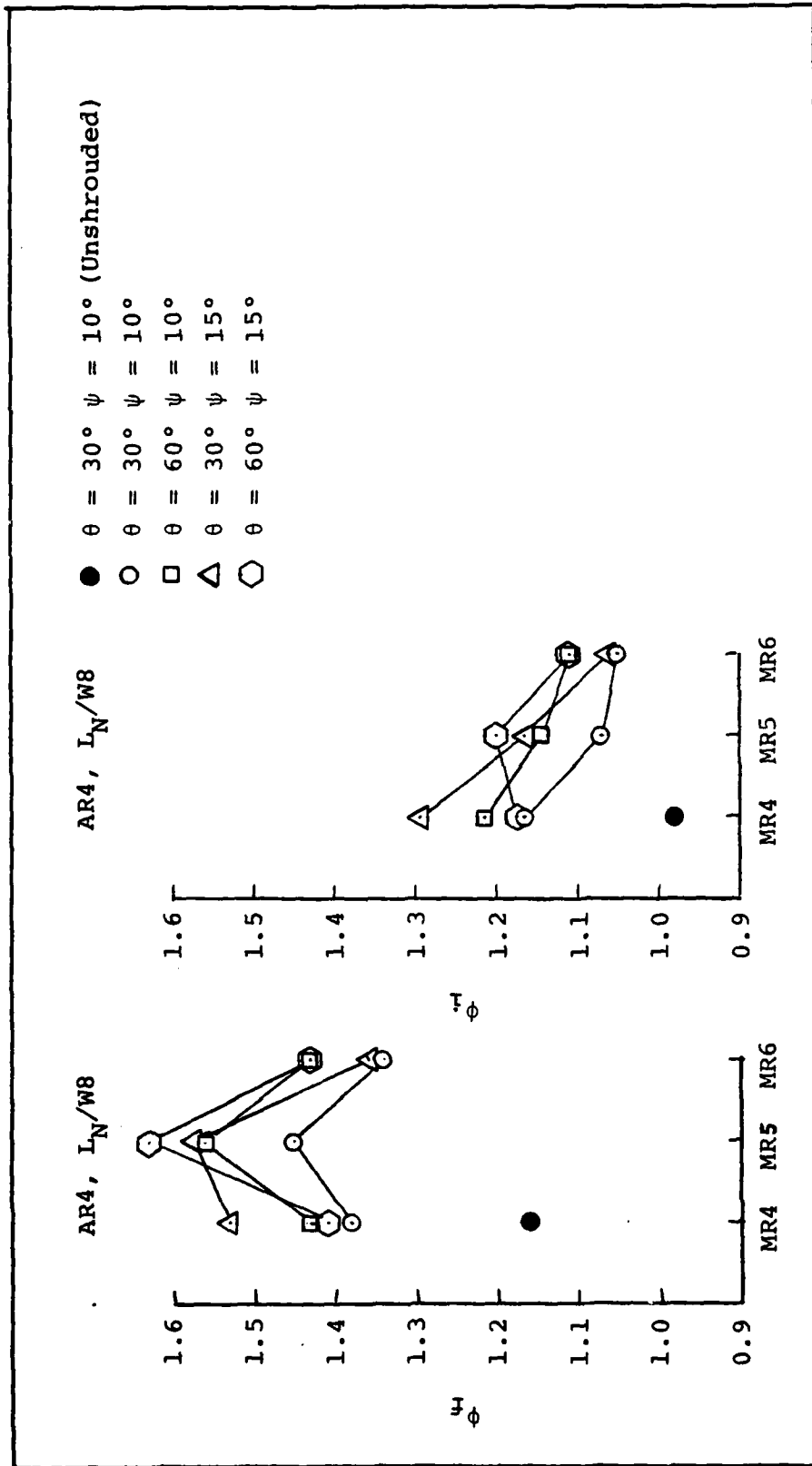


Fig. 28.  $\phi_f$  and  $\phi_i$  vs. MR for AR4  $L_N=1.5$  in (Shrouded)

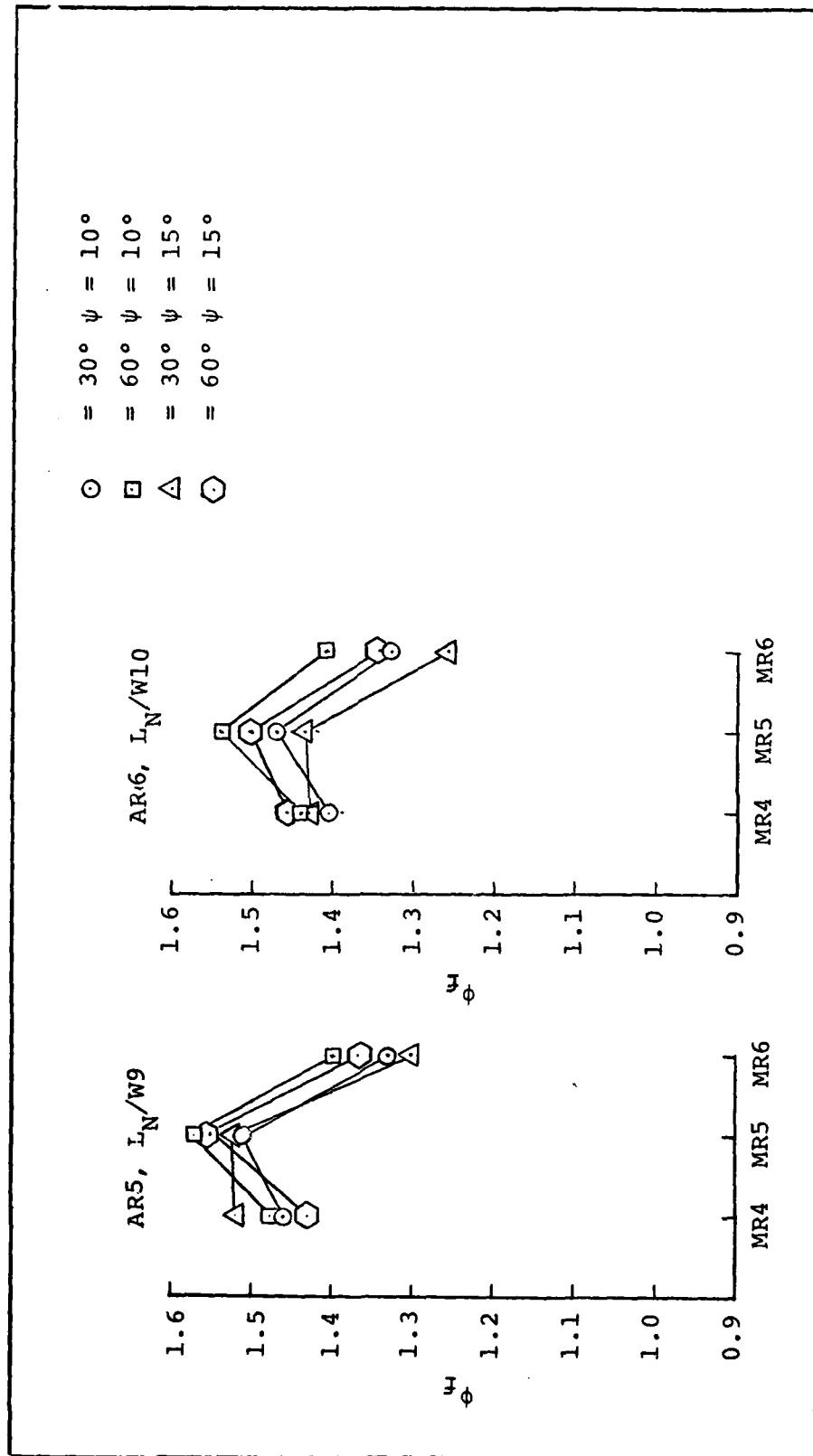


Fig. 29.  $\phi_f$  vs. MR for AR5 and AR6 (Shrouded)

nozzle is the main primary nozzle because of the losses of the Coanda nozzles compared to no-losses in the center nozzle.

#### Ejector's Exit Flow Results

In order to get some idea of mass augmentation and velocity profile at the ejector's exit, measurements for a few configurations were obtained. Two results are shown in Fig. 30, and the nomenclature is shown in Fig. 31. The LHS graphs are from the unshrouded ejector (configuration:  $L_N=0.69$  in,  $\theta=0$  deg,  $\psi=0$  deg, flow distribution in percent, center-Coanda-diffuser 45-50-5 percent,  $m_S/m_P=3.5$ ). The RHS graphs are from the shrouded ejector (configuration:  $L_N=1.5$  in.,  $\theta=0$  deg,  $\psi=10$  deg, flow distribution in percent, center-Coanda-end wall 60-35-5 percent,  $m_S/m_P=5$ ). The influence of the flow phenomena which was discussed earlier, can be seen in these graphs.

The graphs of the unshrouded ejector show:

1. The vortex flow at the ejector's inlet causing two velocity peaks in the Coanda Jet.
2. The high gradients in velocity near the walls, especially for  $h/H=0$ , although the center nozzle jet has the span of the ejector.

The graphs of the shrouded ejector show:

1. The velocities across horizontal line are nearly uniform.

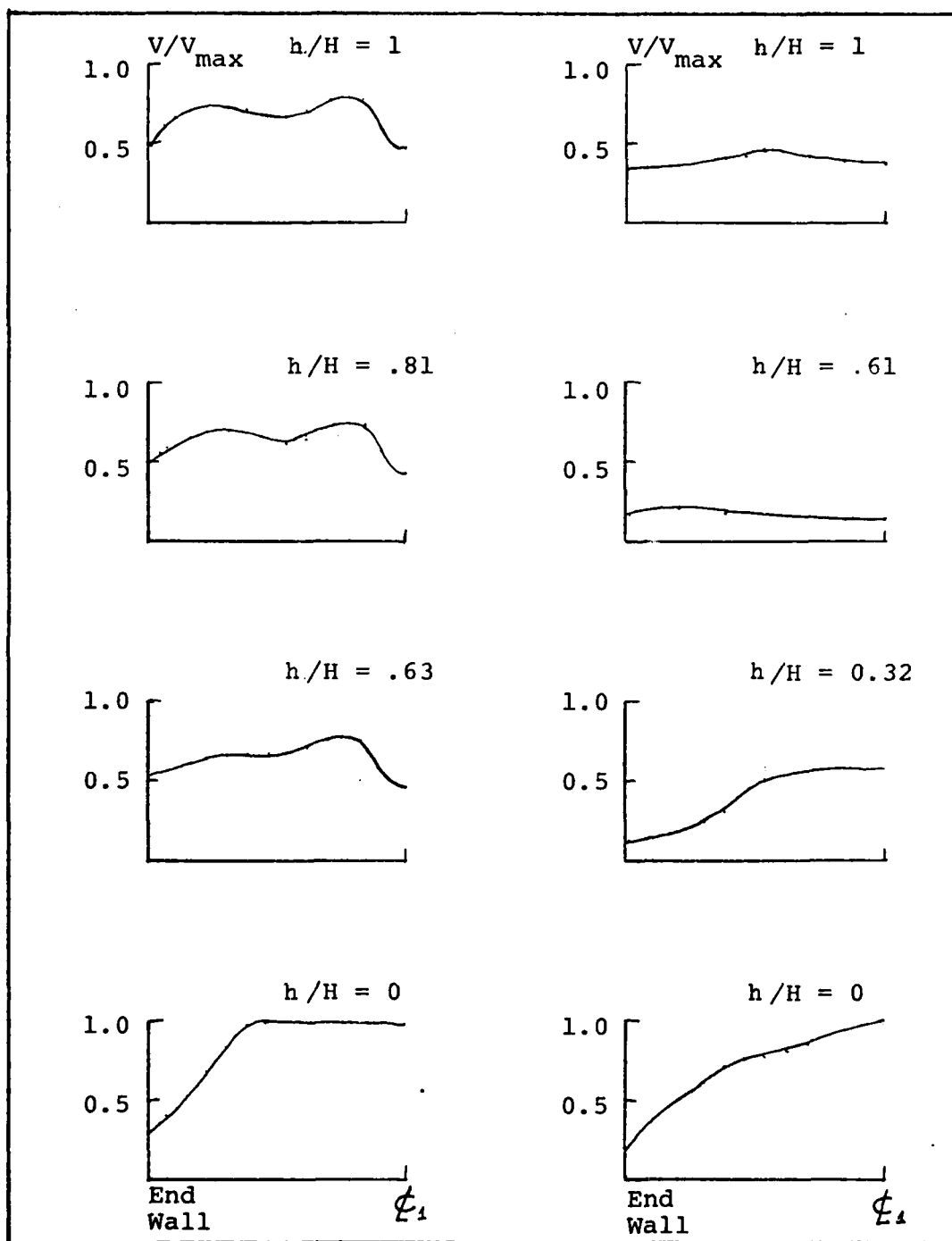


Fig. 30. Velocity Profiles

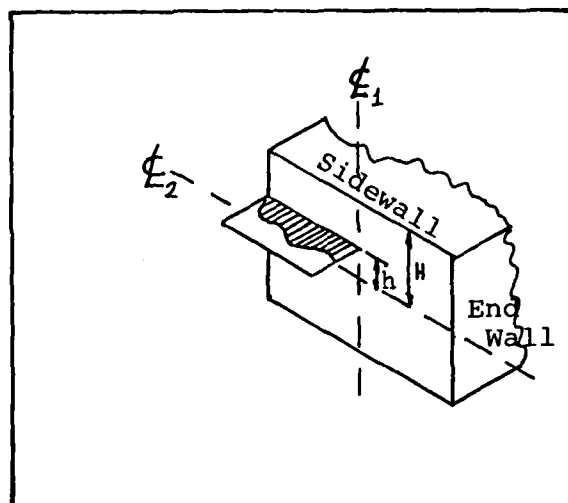


Fig. 31. Nomenclature for Velocity Profile

2. A moderate gradient in velocity at  $h/H=0$  which means less losses. Recall that in this case, the center nozzle jet had a reduced span.

## V. Conclusions and Recommendations

The first part of this chapter deals with conclusions and recommendations obtained in the following:

1. Thrust calibrations of the nozzles.
2. General flow phenomena investigations.
3. Results from the unshrouded and shrouded ejectors.

The second part is a discussion of future experiments suggested from the results of this study.

### Nozzle Thrust Calibrations

1. A rectangular, straight nozzle with a converging plenum, discharging to free surroundings, can be considered isentropic up to 0.8 Mach.

2. The free thrust of a rectangular, flat and thin slotted (0.05 inch and smaller) nozzle discharging air tangential to a wall can be reduced up to 0.7 of the isentropic thrust at the high subsonic Mach number.

3. End-wall nozzles with fan-like jets, have a negligible direct contribution to the thrust, but are very important to maintain an orderly flow, thus increasing the overall thrust.



### General Flow Phenomena Investigation

1. 3-D shroudings at the ejector's inlet and exit are essential for improving thrust augmentation.
2. In a rectangular ejector, end-wall nozzles are essential to prevent thrust-reducing stalls.
3. Although turbulent flow at the ejector inlet enhances flow mixing, the end result could be nonbeneficial to the thrust.

### Results from Unshrouded and Shrouded Ejectors

1. Using the Coanda nozzles as the main primary nozzles results in best thrust performance. The Coanda nozzles should be positioned away (Fig. 32) from the inlet shroud to eliminate the losses due to interaction of high energy flow with the walls. Besides, a jet from a shifted nozzle has two sides to interact with the secondary flow.
2. Reducing the span of the primary nozzle under the span of the ejector can eliminate another source of losses (Fig. 33).
3. End-wall nozzles or other BLC nozzles have a negligible direct contribution on the thrust, since they suffer relatively great losses in their isentropic thrust. On the other hand, they are very important to maintain a stall-free flow which is essential to ejector's performance. Fig. 32 (RHS) shows a method where a vane-like BLC nozzle is extended in the flow. The jet so injected, has

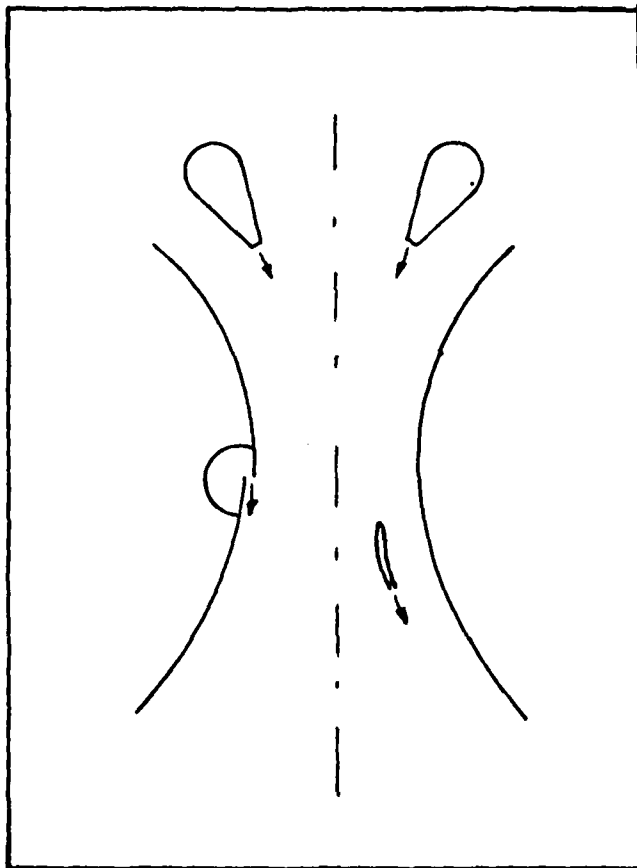


Fig. 32. Two Methods of BLC

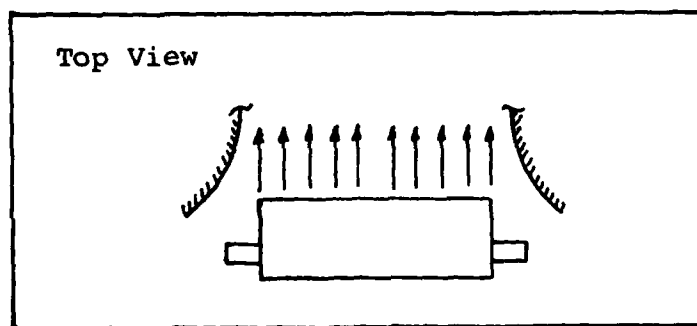


Fig. 33. Reduced Span of Primary Nozzle

the benefits of not being blown tangential to the wall and having two interacting sides with the secondary flow.

4. In a short ejector, part of the thrust is due to direct thrust of part of the primary jets because of inability to be mixed with the secondary flow.

### Discussion of Future Testing

#### Comparison of Ejector's Performances

In order to be able to compare performances of different thrust augmenting ejectors, it is suggested that ejectors will be designed to be attached to a standard apparatus and tested with standard procedures. This method will allow a comparison of performances on the same basis and eliminate differences in experimental methods.

The suggested apparatus shown in Fig. 34 is a pendulum-like pipe to which the ejector is attached to the lower flange.

The detailed test procedures are still to be determined. Two tentative suggestions are:

1. Calculation of the ratio of ejector's thrust to the thrust of a standard L-shaped circular nozzle for the same upstream total pressure and mass flow.

2. Comparison of impulse gained from a given stored energy (e.g., the energy stored in a closed pressurized given volume, between two reference pressures) to the impulse obtained by the standard circular nozzle.

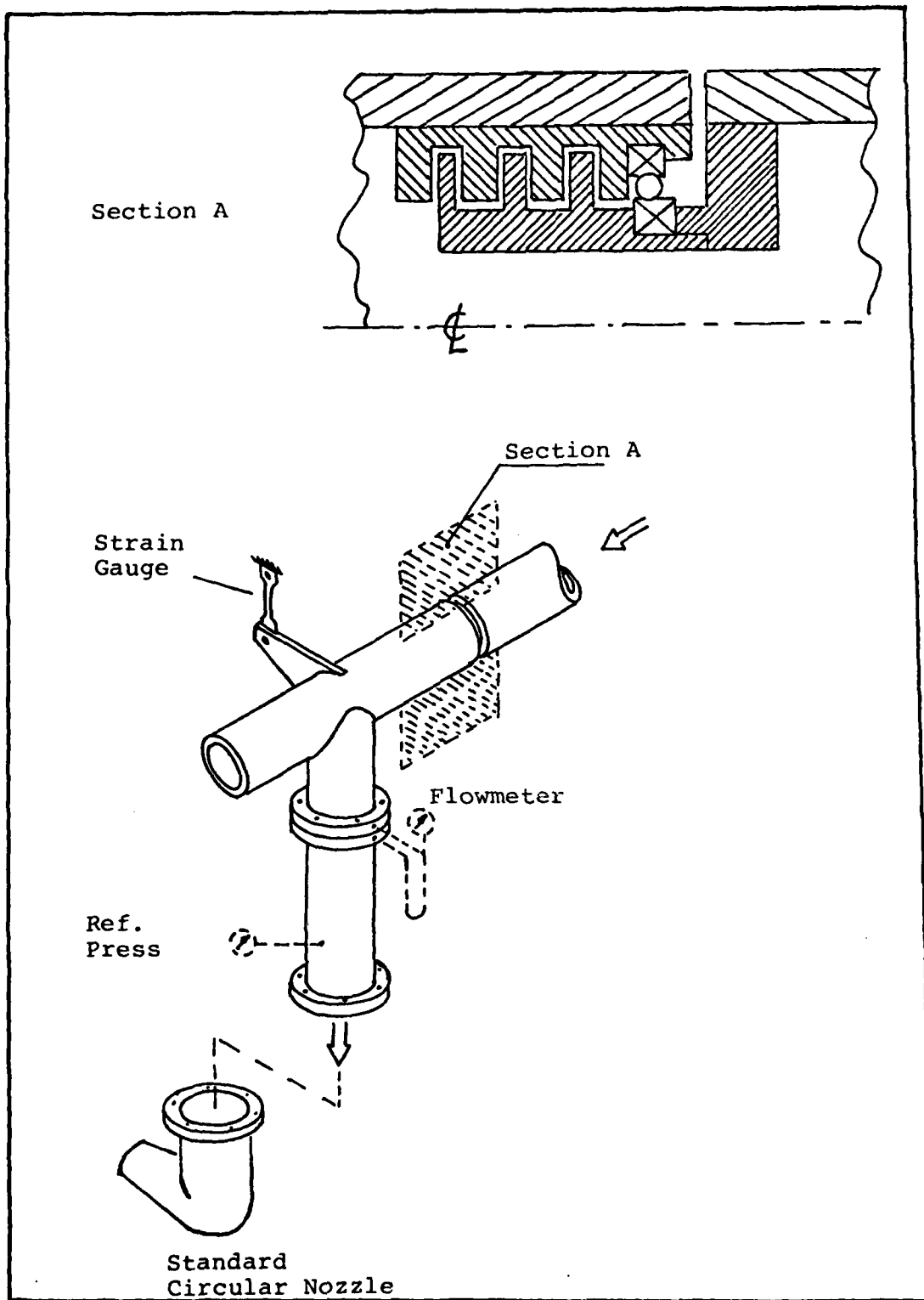


Fig. 34. Standard Test Apparatus--Suggestion

### The Circular Ejector

Thrust augmenting ejectors are generally rectangular in order to incorporate them into a wing of a VTOL aircraft. A circular ejector with annular nozzle (Fig. 35) has some advantages (compared to rectangular) that can make it worthwhile to be considered for a VTOL aircraft.

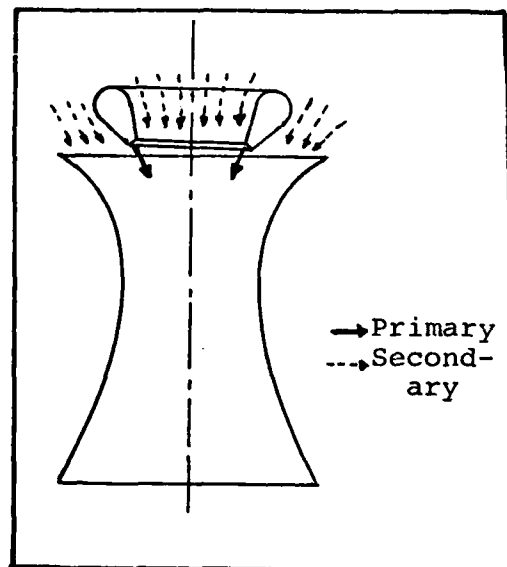


Fig. 35. Circular Ejector

1. The flow is axisymmetric. No 3-D flow phenomena has to be overcome by shrouds and extra nozzles.
2. Flow losses due to ejector wall are minimized because the minimal perimeter for a given cross section is a circle.

An example of application is given in Fig. 36 where two circular ejectors are installed on a fuselage of a canard aircraft. The lift for hovering is generated by the hybrid thrust, meaning that while the exhaust jet is vectored down, the fan pressurized air is supplied to the two ejectors.

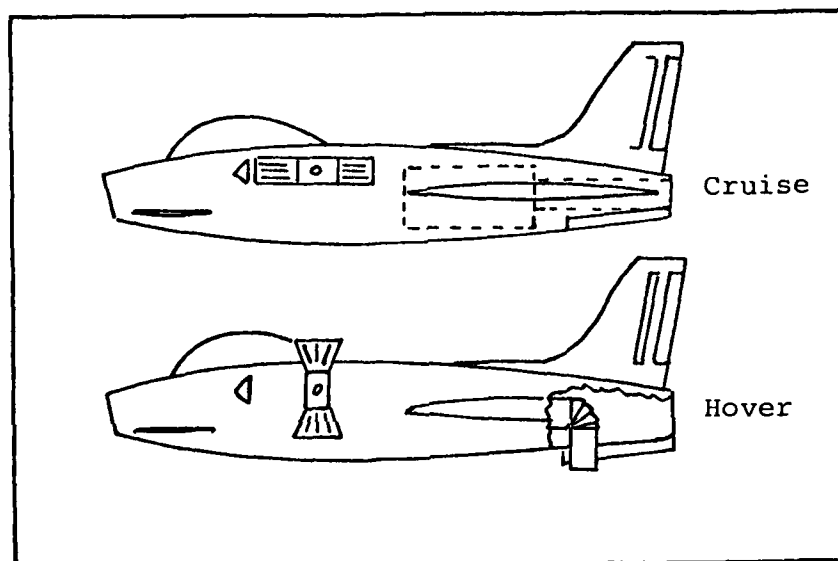


Fig. 36. A Circular Ejector Application

The advantages of such an arrangement in comparison to wing-mounted ejectors are:

1. Decrease in weight.
2. Decrease in flow losses.
3. Safer and simpler transition flight mode.

The reasons for the above are:

1. Lighter material, due to use of relative cold air.

2. No heat isolation is needed.
3. Shorter piping. The fan exit is nearer to the ejectors.
4. Energy losses of the colder air through the shorter pipes are lessened.
5. Simple mechanism for rotating the ejector in transition mode. Wing untouched.

The drag due to the external ejector can be reduced by retractable diameter circular ejector and fairings. Another approach is using the nose segment of the fuselage as a retractable circular ejector (Fig. 37).

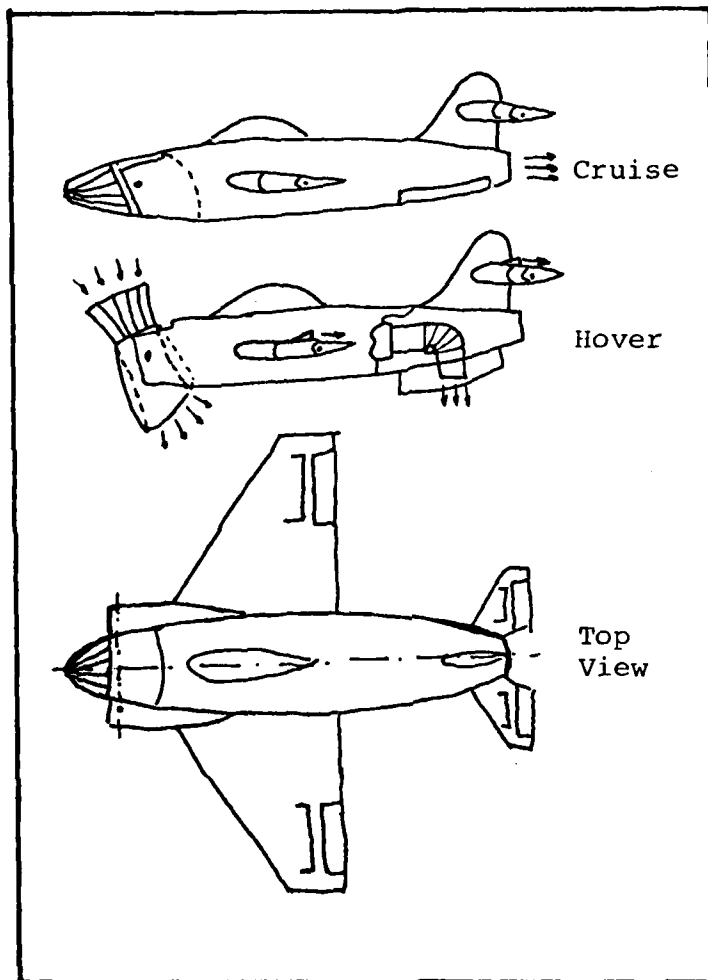


Fig. 37. A Circular Ejector Application



### Bibliography

1. Liepmann, H. W., and Roshko, A. Elements of Aerodynamics. John Wiley & Sons, Inc., 1957.
2. Dean, Jr., W. N. Some Characteristics of a Small Aspect Ratio Ejector. AFIT Thesis, 1978.
3. Flowmeter-Computer Handbook. ASME, 1971.
4. Alperin, M.; Wu, J. J. The Alperin Jet-Diffuser Ejector. Naval Weapons Center, California, 1976.
5. Workshop on Thrust Augmenting Ejectors. AMES Research Center, June 28-29, 1978.
6. O'Donnell, R. M.; and Squyers, R. A. V/STOL Ejector Short Diffuser Study-Final Report. Vought Corporation ATC, Inc., Texas, 1976.
7. Ambrosiani, J. P., and Stewart, V. R. Lift Augmentation Ejectors for V/STOL Aircraft. North American Rockwell, Columbus Division, 1971.
8. Newman, B. G. "The Deflection of Plane Jets by Adjacent Boundaries--Coanda Effect." G. W. Lachmann, Pergamon Press, Vol. 1, 1961.
9. Viets, H. "Thrust Augmenting Ejectors," Lecture Series, Von-Karman Institute for Fluid Dynamics, 1973.

### Appendix A: Primary Flow Calculation

The primary flow calculations were based on the method described in Ref. 3.

The primary flow is obtained by using the following equations:

$$Y_I = K_3 \left( \frac{DPI * 13.57}{(PI + P_a) * C} \right) + 1 \quad (8)$$

$$\rho_I = 2.7 \left( \frac{(P_a + PI) * C}{T_a} \right) \quad (9)$$

$$\dot{m}_{PI} = Y_I * K_4 \sqrt{DPI * \rho_I * 13.57} \quad (10)$$

where the values of the constants are given in Table VI.

TABLE VI  
CONSTANTS FOR PRIMARY FLOW

Nozzle	Pipe Dia. (in)	Orifice Dia. (in)	I	K <sub>3</sub>	K <sub>4</sub>
Center	3.068	1.000	22.99	-0.01071	0.06011
Coanda	3.068	0.750	12.8144	-0.01071	0.03350
Diffuser	2.067	0.500	12.578	-0.01057	0.0149

## Appendix B: Total Flow Calculation Program

The output of program EJECT listed on pages 77, and 78 gives the following properties at the cross section of which the input data was entered:

1. Velocity map.
2. Mass flow.
3. Momentum flux.
4. Skewness factor -  $\beta$ .

The program uses a canned program named IBCIEU from IMSL library which interpolates a 2-D course grid of modal points data--the input data matrix--into a finer grid by using a bi-cubic spline method. Fig. 38 illustrates the two matrices.

### Skewness Factor - $\beta$

The velocity distribution across any cross-section along the ejector is, in general, non-uniform. This non-uniformity may be lumped into a single parameter by the following definition (Ref. 9:17), assuming constant density at the cross section.

$$\hat{\beta} = \frac{\sum_j V_j^2 A_j}{\frac{1}{\sum A_j} \sum_j V_j A_j}^2 \quad (11)$$

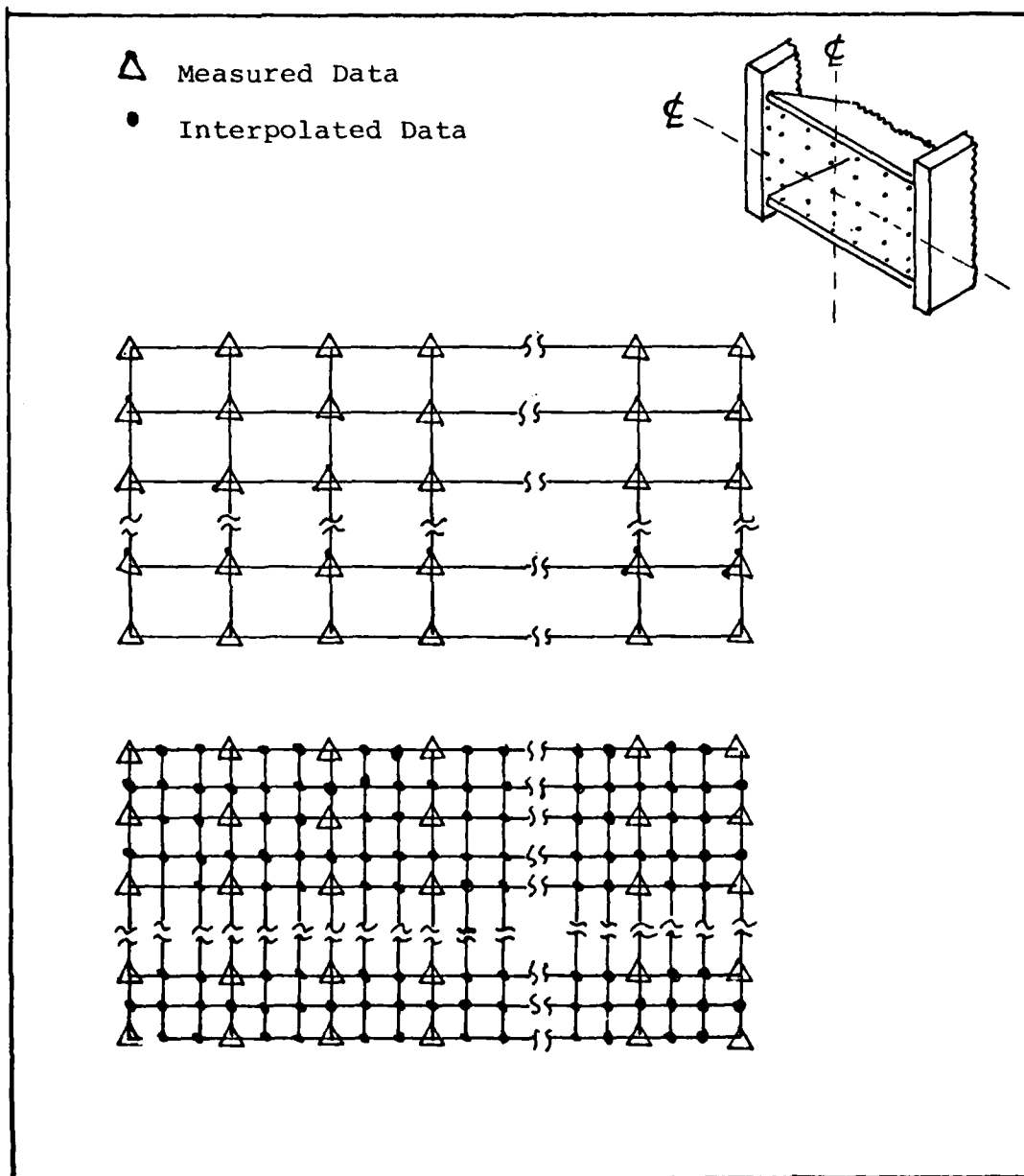


Fig. 38. Coarse and Fine Data Matrices

Eq. (11) means that  $\beta$  is the ratio of momentum flux through the cross section, to momentum flux due to a uniform average velocity.

For reasons of clarity, the  $\beta$  in program EJECT is calculated as follows:

$$\beta = (\hat{\beta} - 1) * 1000 \quad (12)$$

Program EJECT--User's Manual

The following sequence of cards should be used for program EJECT:

JOB CARD

CONTROL CARDS

ATTACH, LIB, IMSL, ID = LIBRARY, SN = ASD.

LIBRARY, LIB.

FTN

LGO

7/8/9

PROGRAM DECK (Listed on pages 74, 75, 76)

7/8/9

DATA DECK

CARD #1 [I-integar, R-real]

RUN #(I), AMB. PRESS.- PSIA (R),

TEMP at cross section-RANKIN (R),

STATIC PRESS. at cross section-

PSIA (R)

CARD #2 Number of horizontal scans (I),  
location in inches of first  
(upper) scan, location of second  
scan, etc. (R).

CARD #3A Number of increments between  
first and second scan (I).

CARD #3B Number of increments between  
second and third scan (I).

(Note: Number of #3 Cards should  
be the number of the horizontal  
scan minus 1.)

CARD #4A P11, P12, P13, etc.

CARD #4B P21, P22, P23, etc.

(Note: PIJ is the gauge total  
pressure of the nodal points of  
the cross section, expressed in  
inches of water.)

Example of an output is shown in Figs. 39 and 40.

#### Output Explanation

INPUT DATA (Coarse Matrix). The left column is  
the vertical location of the horizontal scans (in inches).  
The other eleven columns are the total pressures (in-water  
gauged) at the nodal points. The horizontal station of  
the nodal points are (from left to right, in inches)  
-3.25, -2.75, -2, -1.25, -0.625, 0, 0.625, 1.25, 2, 2.75,  
3.25.

```

      PROGRAM EJECT (INPUT,OUTPUT,TAPE5=INPUT,TAPE6=OUTPUT)
      DIMENSION X(9),Y(11),F(9,11),FL(40,29),WK(210)
      DIMENSION XL(40),YL(29),FF(9,11),IFL(40,29)
C     FORMATS FOR PROGRAM.
100    FORMAT (F6.2,3X,11F7.2)
200    FORMAT (F6.2,2X,15F7.2)
210    FORMAT (F6.2,2X,14F7.2)
300    FORMAT (F6.2,3X,15I3)
      10 CONTINUE
      MEZ=1
C     INPUT CONSTANTS FOR CURRENT RUN
      PRINT*, "CONSTANTS FOR CURRENT RUN"
      PRINT*, "RUN NO., P-AMB(PSIA), TEMP(R), P-STAT(PSIA)"
      READ*,NRUN,PAMB,TEMP,PSTAT
      IF (EOF(5LINPUT).NE.0.0) STOP
C     ZEROING ALL DATA IN MATRICES
      DO 6 I=1,9
      DO 6 J=1,11
6       F(I,J)=0.
      DO 7 I=1,40
      DO 7 J=1,29
7       FL(I,J)=0.
C     VERTICAL LOCATION OF HORIZANTEL POINTS INTO VECTOR
C     Y( ) AND YL( )
      NY=11
      DATA Y/-3.25,-2.75,-2.,-1.25,-0.625,0.0,0.625,1.25,
      12.,2.75,3.25/
      NYL=29
      DATA YL/-3.25,-3.125,-3.,-2.875,-2.75,-2.5,-2.25,-2.
      1,-1.75,-1.5,-1.25,-.9375,-.625,-.3125,0.,.3125,
      1.625,.9375,1.25,1.5,1.75,2.,2.25,2.5,2.75,2.875,3.,
      13.125,3.25/
C     LOCATION OF HORIZANTEL SCANS INTO VECTOR X( )
      PRINT*, "NO. OF HORIZANTEL LINES, LOCATIONS(INCH)"
      READ*,NX,(X(I),I=1,NX)
C     LOCATION FOR HORIZANTEL INCREMENTS INTO VECTOR XL( )
      K=0
      DO 30 I=2,NX
      IM1=I-1
      PRINT*, "HOW MANY INCREMENTS BETWEEN LINES ",IM1,"
      1 AND ",I,"="
      READ*,INC
      FINC=FLOAT(INC)
      DINC=(X(I)-X(IM1))/FINC
      FK=0.
      DO 40 II=1,INC
      K=K+1
      XL(K)=X(IM1)+FK*DINC
40      FK=FK+1.
30      CONTINUE
      K=K+1
      XL(K)=X(NX)
      NXL=K
C     INPUT TABULAR DATA INTO F(I,J)
      PRINT*, "INPUT IN FOLLOWING POINTS H+ IN WATER-IN"
      DO 50 I=1,NX
      READ*,(F(I,J),J=1,11)
50      CONTINUE

```



```

: C PRINTING OUT THE GIVEN DATA
:716 PRINT*, " "
: PRINT*, " "
: PRINT*, "***** OUTPUT FOR RUN ", NRUN, " *****"
: PRINT*, "INPUT DATA "
: DO 16 I=1, NX
:16 WRITE(6,100)X(I), (F(I,J), J=1,11)
: C TRANSLATING THE DATA IN F( ) TO VELOCITY(FT/SEC)
: DO 90 I=1, NX
: DO 95 J=1,11
: PTOT=F(I,J)+3.61E-2+PAMB
:95 F(I,J)=SQRT(7.+1715.+TEMP*((PTOT/PSTAT)+0.2857-1.))
:90 CONTINUE
: C CREATING A SYMMETRIC MATRIX
: NXX=(NX-1)/2
: DO 21 I=1, NXX
: DO 22 J=1,5
: FF(I,J)=(F(I,J)+F(I,12-J)+F(NX+1-I,J)+F(NX+1-I,12-
: 1J))*0.25
: FF(I,12-J)=FF(I,J)
: FF(NX+1-I,J)=FF(I,J)
: FF(NX+1-I,12-J)=FF(I,J)
:22 CONTINUE
:21 CONTINUE
: FF(NXX+1,6)=F(NXX+1,6)
: DO 23 I=1, NXX
: FF(I,6)=(F(I,6)+F(NX+1-I,6))*0.5
: FF(NX+1-I,6)=FF(I,6)
:23 CONTINUE
: DO 24 J=1,5
: FF(NXX+1,J)=(F(NXX+1,J)+F(NXX+1,12-J))*0.5
:24 FF(NXX+1,12-J)=FF(NXX+1,J)
: C PRINTING OUT TRANSLATED DATA
: PRINT*, "TRANSLATED DATA INTO VELOCITIES (FT/SEC)"
: DO 17 I=1, NX
:17 WRITE(6,100)X(I), (F(I,J), J=1,11)
: PRINT*, "TRANSLATED SYMMETRIC DATA"
: DO 62 I=1, NX
:62 WRITE(6,100)X(I), (FF(I,J), J=1,11)
: C USING ***IBCIU*** TO CALCULATE THE FINER MATRIX
: IFD=9
: IFLD=40
: CALL IBCIU(F, IFD, X, NX, Y, NY, XL, NXL, YL, NYL, FL, IFLD,
: 1WK, IER)
: PRINT*, "IER=", IER
: C PRINTING OUT REFINED MATRIX
: PRINT*, "REFINED MATRIX LEFT SIDE AND C.L."
: DO 19 I=1, NXL
:19 WRITE(6,200)XL(I), (FL(I,J), J=1,15)
: PRINT*, "REFINED MATRIX RIGHT SIDE"
: DO 20 I=1, NXL
:20 WRITE(6,210)XL(I), (FL(I,J), J= 16,29)
: C CALCULATION OF MASS FLOW, MOMENTUM FLUX AND BETA
:400 FLOW=0.
: FLUX=0.
: RO=(PSTAT+144.)/(1715.+TEMP)
: DO 110 I=2, NXL
: DO 120 J=2,29

```

```

:      AVEL=(FL(I-1,J-1)+FL(I-1,J)+FL(I,J-1)+FL(I,J))*0.25
:      AREA=(XL(I)-XL(I-1))* (YL(J)-YL(J-1))/144.
:      FLOW=FLOW+(RD*AREA*AVEL)
:      FLUX=FLUX+(RD*AREA*AVEL**2)
:120  CONTINUE
:110  CONTINUE
:      TAREA=6.50*(X(NX)-X(1))/144.
:      RD=(PSTAT*144.)/(1715.*TEMP)
:      WAVE=FLOW/(RD*TAREA)
:      BETA=(FLUX/(RD*WAVE**2*TAREA)-1.)*1000.
:      FLOW=FLOW*32.2
:      PRINT*," "
:      PRINT*,"AMB. PRESS. (PSIA)=",PAMB
:      PRINT*,"TEMP. AT CROSS SEC. (R-DEG)=",TEMP
:      PRINT*,"STATIC PRESS. AT CROSS SEC. (PSIA)=",PSTAT
:      PRINT*," "
:      TAREA=TAREA*144.
:      PRINT*,"CROSS SECTION AREA (SQ. IN.)=",TAREA
:      PRINT*,"MASS FLOW (LBM/SEC)=",FLOW
:      PRINT*,"MOMENTUM FLUX (LBF)=",FLUX
:      PRINT*,"BETA=",BETA
:      PRINT*," "
:      PRINT*," "
:      IF(MEZ.EQ.2) GO TO 500
:      CALL IBCIEU(FF,IFD,X,NX,Y,NY,XL,NXL,YL,NYL,FL,IFLD
:1,WK,IER)
:      PRINT*,"IER=",IER
:      PRINT*,"REFIND SYMMETRIC MATRIX RIGHT SIDE AND C.L."
:      DO 25 I=1,NXL
:25  WRITE(6,200)XL(I),(FL(I,J),J=1,15)
:      MEZ=2
:      GO TO 400
: C  NORMALIZING THE SYMMETRIC MATRIX FL( ) TO 10 INTEGERS
:500  VMAX=0.
:      VMIN=1.E6
:      DO 51 I=1,NXL
:      DO 51 J=1,29
:      IF(FL(I,J).GT.VMAX)VMAX=FL(I,J)
:51  IF(FL(I,J).LT.VMIN)VMIN=FL(I,J)
:      DV=VMAX-VMIN
:      DO 26 I=1,NXL
:      DO 27 J=1,29
:      VNOR=(FL(I,J)-VMIN)*(10./DV)
:      BVNOR=VNOR+0.5
:      IVNOR=INT(BVNOR)
:27  IFL(I,J)=IVNOR
:26  CONTINUE
:      PRINT*,"NORMALIZED MATRIX"
:      DO 28 I=1,NXL
:28  WRITE(6,300)XL(I),(IFL(I,J),J=1,15)
:      GO TO 10
:      END
:
:♦EOR
:♦EOR
:♦EOF

```

Fig. 39. Program EJECT Output

AMB. PRESS. (PSIA)=14.4  
 TEMP. AT CROSS SEC. (R-DEG)=530.  
 STATIC PRESS. AT CROSS SEC. (PSIA)=14.4

CROSS SECTION AREA (SQ. IN.)=26.52  
 MASS FLOW (LBM/SEC)=1.558310889536  
 MOMENTUM FLUX (LBF)=6.794637790581  
 BETA=218.9937/87579

IER=0

REFINED SYMMETRIC MATRIX RIGHT SIDE AND C.L.

0.00	101.00	106.74	112.04	116.48	119.61	121.63	121.56	124.27	132.59	141.24	142.92	129.84	114.81	112.51	114.81
.79	54.34	62.36	69.78	75.42	78.37	75.06	64.65	54.37	43.71	49.29	50.00	49.17	47.72	47.49	47.72
1.39	42.35	47.25	52.00	56.42	60.35	67.27	77.11	95.38	124.72	156.20	178.05	181.56	174.83	175.42	176.05
2.04	52.73	54.81	59.35	67.55	81.22	126.52	180.80	223.90	241.36	243.22	240.52	257.23	233.58	309.24	313.60
2.69	42.35	47.25	52.00	56.42	60.35	67.27	77.11	95.38	124.72	156.20	178.05	181.56	174.83	175.42	176.05
3.29	54.34	62.36	69.78	75.42	78.37	75.06	64.65	54.37	43.71	49.29	50.00	49.17	47.72	47.49	47.72
4.00	101.00	106.74	112.04	116.48	119.61	121.63	121.56	124.27	132.59	141.24	142.92	129.84	114.81	112.51	114.81

AMB. PRESS. (PSIA)=14.4  
 TEMP. AT CROSS SEC. (R-DEG)=530.  
 STATIC PRESS. AT CROSS SEC. (PSIA)=14.4

CROSS SECTION AREA (SQ. IN.)=26.52  
 MASS FLOW (LBM/SEC)=1.558310889536  
 MOMENTUM FLUX (LBF)=6.793691159112  
 BETA=218.723362022

NORMALIZED MATRIX

0.00	2	2	3	3	3	3	3	3	3	3	3	3	3	3	3
.79	0	1	1	1	1	1	1	0	0	0	0	0	0	0	0
1.39	0	0	0	1	1	1	1	2	3	4	5	5	5	5	3
2.04	0	0	1	1	1	3	5	7	7	8	8	9	10	10	10
2.69	0	0	0	1	1	1	1	2	3	4	5	5	5	5	5
3.29	0	1	1	1	1	1	1	0	0	0	0	0	0	0	0
4.00	2	2	3	3	3	3	3	3	3	4	4	3	3	3	3

CONSTANTS FOR CURRENT RUN  
 RUN NO., P-AMB(PSIA), TEMP(R), P-STAT(PSIA)

Fig. 40. Program EJECT Output

TRANSLATED DATA INTO VELOCITIES (FT/SEC). The same as the INPUT DATA, but the pressures are translated into velocities.

TRANSLATED SYMMETRIC DATA. The same as the TRANSLATED DATA INTO VELOCITIES, but averaging all four symmetric modal points to one value.

REFINED MATRIX LEFT SIDE and C.L. The left column is the location of the given and interpolated horizontal scans (in inches). The other fifteen columns are the given and interpolated velocities for the following horizontal stations (left to right, in inches): -3.25, -3.125, -3, -2.875, -2.75, -2.5, -2, -1.75, -1.5, -1.25, -0.9375, -0.675, -0.3125, 0.

REFINED MATRIX RIGHT SIDE. The same as REFINED MATRIX LEFT SIDE, but for the following horizontal stations (left to right, in inches): 0.3125, 1.675, 0.9375, 1.25, 1.5, 1.75, 2, 2.25, 2.5, 2.75, 2.875, 3, 3.125, 3.25.

The given pressures, temperature, mass flow, momentum flux, and BETA are self-explanatory.

REFINED SYMMETRIC MATRIX LEFT SIDE and C.L. Transferring the fine given matrix into a symmetric matrix, by averaging every four symmetric nodal points.

NORMALIZED MATRIX. The normalized matrix was generated from REFINED SYMMETRIC MATRIX LEFT SIDE and C.L. as follows: The lowest velocity was given the value 0, the highest velocity was given the value 10. The range

between these two velocities was divided to 11 increments. Each velocity in the matrix was assigned a value between 0 and 10 according to the increment it was in. The result is the "sky-line" of the velocity's profile.

## VITA

Eli Kedem was born in Haifa, Israel, on 21 October 1939. After completing high school, he attended the Technical School of the IAF (Israeli Air Force), and became an aircraft mechanic. In the years 1958-1969, he served in IAF as a mechanic and technical instructor. In the years 1969-1973, he studied in the Technion--Institute of Technology, Haifa, Israel, and received his B.Sc. in Mechanical Engineering. He continued to serve in the IAF as a Headquarters Officer and an engineer.

On June 1978 he entered the AFIT Graduate School.

Permanent Address: 25 Reading Street  
Tel-Aviv, Israel

UNCLASSIFIED

SECURITY CLASSIFICATION OF THIS PAGE (When Data Entered)

REPORT DOCUMENTATION PAGE		READ INSTRUCTIONS BEFORE COMPLETING FORM
1. REPORT NUMBER AFIT/GAE/AA/79D 7	2. GOVT ACCESSION NO.	3. RECIPIENT'S CATALOG NUMBER
4. TITLE (and Subtitle)  AN EXPERIMENTAL STUDY OF STATIC THRUST AUGMENTATION USING A 2-D VARIABLE EJECTOR		5. TYPE OF REPORT & PERIOD COVERED  MS Thesis
		6. PERFORMING ORG. REPORT NUMBER
7. AUTHOR(s)  ELI KEDEM		8. CONTRACT OR GRANT NUMBER(s)
9. PERFORMING ORGANIZATION NAME AND ADDRESS  Air Force Institute of Technology (AFIT-EN) Wright-Patterson AFB, Ohio 45433		10. PROGRAM ELEMENT, PROJECT, TASK AREA & WORK UNIT NUMBERS
11. CONTROLLING OFFICE NAME AND ADDRESS		12. REPORT DATE  December 1979
		13. NUMBER OF PAGES  93
14. MONITORING AGENCY NAME & ADDRESS (if different from Controlling Office)		15. SECURITY CLASS. (of this report)  Unclassified
		15a. DECLASSIFICATION/DOWNGRADING SCHEDULE
16. DISTRIBUTION STATEMENT (of this Report)  Approved for public release; distribution unlimited		
17. DISTRIBUTION STATEMENT (of the abstract entered in Block 20, if different from Report)  JOSEPH P. HIPES, Major, USAF Director of Public Affairs		
18. SUPPLEMENTARY NOTES		
19. KEY WORDS (Continue on reverse side if necessary and identify by block number)  Ejectors Thrust Augmentation V/STOL		
20. ABSTRACT (Continue on reverse side if necessary and identify by block number)  A short rectangular throat ejector was constructed and tested to determine the effects of a number of variables on thrust augmentation and mass augmentation. The variables included those associated with geometry (e.g., diffuser length/throat length, diffuser area ratio, diffuser sidewall angle, nozzle angles and positions) and those due to differences in primary mass flow rate distributions among the nozzles. There were two kinds of thrust augmentation that were calculated; the free		

DD FORM 1473

1 JAN 73

EDITION OF 1 NOV 65 IS OBSOLETE

UNCLASSIFIED

SECURITY CLASSIFICATION OF THIS PAGE (When Data Entered)



AD-A079 857

AIR FORCE INST OF TECH WRIGHT-PATTERSON AFB OH SCHOOL--ETC F/G 21/8  
AN EXPERIMENTAL STUDY OF STATIC THRUST AUGMENTATION USING A 2-D--ETC(U)  
DEC 79 E KEDEM  
AFIT/8AE/AA/79D-7

UNCLASSIFIED

NL

2 of 2

40  
40986-7



END

DATE

FILED

3 -80

DOC

UNCLASSIFIED

SECURITY CLASSIFICATION OF THIS PAGE (When Data Entered)

↓  
thrust augmenting ratio and the isentropic thrust augmenting ratio. The free thrust augmenting ratio is the ratio of the ejector's measured thrust to the sum of the nozzles' measured thrust, if each of them were discharged separately to ambient pressure. The isentropic thrust augmenting ratio is the ratio of the ejector's measured thrust to the calculated thrust of the nozzles if discharged isentropically to the ambient pressure.

A free thrust augmenting ratio as high as 1.63 and an isentropic thrust augmenting ratio of up to 1.29 were obtained. Mass augmentation which is the ratio of secondary flow to primary flow was in the range of 3.5 to 5. Some conclusions concerning design aspects were drawn also. They include the necessity of 3-D shrouding for the ejector's inlet and exit and the prevention of blowing high velocity air (primary and BLC flow) tangential to the ejector walls.  
↑

UNCLASSIFIED

SECURITY CLASSIFICATION OF THIS PAGE (When Data Entered)